Electronic Supplementary Material (ESI) for Chemical Science.

Supplementary Information for

Oxidation triggers guest dissociation during reorganization of from an $Fe^{II}_4L_6$ twisted parallelogram

Alex J. Plajer,[†] Felix J. Rizzuto,[†] Larissa K. S. von Krbek, Yohan Gisbert,
Víctor Martínez-Agramunt and Jonathan R. Nitschke

[†]These authors contributed equally.

Correspondence to: jrn34@cam.ac.uk

Table of Contents

1. Materials and methods

All reagents were purchased from commercial sources and used as received. For electrochemical experiments, dry solvents were purchased from Sigma-Aldrich and purged with argon before use. nBu_4NPF_6 was recrystallised three times from ethanol before use. 2-Nitrosopyridine,[1] (4-aminophenylene)-ferrocene[2] **B** and bis(4-aminophenylene)-ferrocene[3] **A** were synthesized according literature procedures. Note that **B** readily oxidised in the presence of air (over the course of several weeks), and was thus stored in a glove-box when not in use.

Nuclear Magnetic Resonance (NMR): NMR spectra were recorded using a 400 MHz Avance III HD Smart Probe (routine ^{1}H NMR), DCH 500 MHz dual cryoprobe (high-resolution ^{13}C and 2D experiments), DPX S5 500 MHz BB ATM (variable temperature NMR) and 500 MHz TCI-ATM cryo NMR spectrometers. Chemical shifts for ^{1}H, ^{13}C and ^{19}F are reported in ppm on the δ scale; ^{1}H and ^{13}C were referenced to the residual solvent peak. Coupling constants (*J*) are reported in hertz (Hz). The following abbreviations are used to describe signal multiplicity for ^{1}H, ^{13}C and ^{19}F NMR spectra: s: singlet, d: doublet, t: triplet, dd: doublet of doublets; dt: doublet of triplets; m: multiplet, b: broad. ^{1}H DOSY NMR experiments were performed on a Bruker 400 MHz Avance III HD NMR. Maximum gradient strength was 6.57 G/cm A. The standard Bruker pulse program, ledbpgp2s, employing a stimulated echo and longitudinal eddy-current delay (LED) using bipolar gradient pulses for diffusion using 2 spoil gradients was utilised. Rectangular gradients were used with a total duration of 1.5 ms. Gradient recovery delays were 875-1400 µs. Individual rows of the S4 quasi-2D diffusion databases were phased and baseline corrected.

Mass spectrometry: Low resolution electrospray ionisation (LR-ESI) mass spectrometry was undertaken on a Micromass Quattro LC mass spectrometer (cone voltage 10-30 V; desolvation temp. 313 K; ionization temp. 313 K) infused from a Harvard syringe pump at a rate of 10 µL min^{-1}. High resolution electrospray ionisation mass spectrometry (HRMS-ESI) was performed on a Waters LCT Premier Mass Spectrometer featuring a Z spray source with electrospray ionisation and modular LockSpray interface.

UV-Vis spectroscopy: UV-Visible absorption spectroscopy was performed using a Perkin Elmer Lambda 750 UV-Vis-NIR spectrophotometer fitted with a PTP-1 Peltier temperature controller accessory. Spectra were obtained in double beam mode using only the (front) analyte beam to record spectra, with air in the (rear) reference path. A background spectrum of the neat solvent was recorded using the analyte beam prior to each experiment and baseline correction applied using the Perkin Elmer WinLab software suite. Samples were analysed using quartz cuvettes with optical path lengths of 10 mm.

Cyclic voltammetry: Solution state cyclic voltammetry (CV) was performed using a BioLogic SP-150 potentiostat with ferrocene (Fc) as an internal reference. Measurements were conducted under an Ar atmosphere using a conventional three-electrode cell: a glassy carbon working electrode, a Pt wire auxiliary electrode, and a Ag/Ag$^+$ quasi-reference electrode. A 0.1 M nBu_4NPF_6/CH_3CN electrolyte was used, with scan rates in the range 25-1000 mV s^{-1}.

Spectroelectrochemistry: Electronic spectra were obtained *in situ* using an Optically Semi-Transparent Thin-Layer Electrosynthetic (OTTLE) cell (path length 0.1 mm) accommodating the Pt counter and Ag/Ag$^+$ reference electrodes, which were separated from the solution by salt bridges containing 0.3 M nBu_4NPF_6/CH_3CN electrolyte. A Pt gauze working electrode (70% transmittance) was located centrally in the optical beam in the lower section of the cell. All solutions were purged with Ar prior to transferral into the OTTLE cell. Potentials were controlled by a BioLogic SP-150 potentiostat, and absorption spectra recorded at regular intervals over the range 250-800 nm. The attainment of a steady-state spectrum and the decay of the current to a constant minimum were taken as being indicative of the complete conversion of the starting material.

Molecular modelling; Molecular model simulations (MM3 force fields) SCIGRESS version FJ 2.6 (EU 3.1.9) Build 5996.8255.20141202.

2. Synthesis and characterisation of 1

Bis(4-(aminophenylene))-ferrocene **A** (6.0 mg, 16 µmol), 2-pyridinecarboxaldehyde (3.5 mg, 10 µmol) and $Fe(PF_6)_2(CH_3CN)_6$ (6.4mg, 10.3 µmol) were dissolved in 1 ml CH_3CN and transferred into a J. Young tube. The purple solution was subjected to three freeze-pump-thaw cycles under and N_2 atmosphere and then heated at 60 °C over 16 h. After cooling to room temperature the purple solution was added to 10 ml Et_2O to precipitate the product. The precipitate was collected by centrifugation and dried *in vacuo*. Yield (10mg, 85%, 2.2 µmol).

^{1}H NMR (CD_3CN, 700 MHz, 298K): δ[ppm] = 9.41 (s), 9.32 (s), 9.28 (s), 9.13 (s), 8.84 (s), 8.62-8.51 (m), 8.45 (d, *J* = 6.3 Hz), 8.39 (d, *J* = 5.6 Hz), 8.29 (d, *J* = 6.4 Hz), 8.28 -8.20 (m), 8.12 (d, *J* = 7.7 Hz), 8.05 (d, *J* = 6.4 Hz), 7.97 (d, *J* = 6.6 Hz), 7.95 (t, *J* = 5.6 Hz), 7.85 – 7.72 (m), 7.73 – 7.65 (m) 7.64 – 7.60 (m), 7.57 (s), 7.57 – 7.50 (m), 7.48 (d, *J* = 5.6 Hz), 7.46 – 7.42 (m), 7.42 – 7.35 (m), 7.31 (d, *J* = 8.2 Hz), 7.27 – 7.20 (m), 7.24 – 7.13 (m), 7.02 (d, *J* = 7.3 Hz), 6.96 (s), 6.75 (bs), 6.66 (d, *J* = 8.4 Hz), 6.57 (s), 6.48 (d, *J* = 9.0 Hz), 6.42 (d, *J* = 7.8 Hz), 6.15 (s,), 6.02 (s), 5.39 (d, *J* = 9.0 Hz), 4.81 (s), 4.70 (s), 4.65 (s), 4.57 (d, *J* = 3.1 Hz), 4.38 (s), 4.35 (s), 4.25 (s), 4.22 (s), 4.19 (s), 4.16 (s), 4.10 (s), 3.91 (s), 3.75 (s), 3.71 (s), 3.43 (s), 3.30 (s), 3.13 (s), 2.53 (s), 2.48 (s); see figure below for signal assignment.

^{13}C NMR (CD_3CN, 176 MHz, 298K): δ[ppm] = 175.00, 173.98, 173.14, 171.27, 169.60, 164.81, 159.55, 158.49, 158.26, 158.20, 158.12, 157.98, 157.73, 157.16, 156.91, 156.75, 156.58, 156.24, 155.17, 149.26, 148.46, 145.10, 144.89, 143.95, 141.37, 140.67, 140.63, 140.58, 140.39, 140.29, 140.12, 139.63, 139.07, 138.47, 138.44, 138.05, 131.44, 131.38, 130.64, , 129.76, 129.28, 129.09, 129.03, 128.82, 128.72, , 128.28, 128.10, 127.05, 126.89, 126.55, 126.42, 126.06, 125.79, 125.68, 125.46, 124.57, 124.22, 121.67, 121.45, 121.25, 120.89, 120.58, 85.02, 83.97, 83.75, 83.52, 82.61, 78.15, 77.96, 77.77, 76.85, 75.38, 75.19, 73.89, 72.47, 72.42, 71.87, 71.34, 71.25, 71.02, 70.84, 70.53, 70.44, 70.09, 69.76, 69.44, 68.75, 67.75, 65.97, 65.67, 65.40, 64.70, 64.37, 63.67

^{19}F NMR (CD_3CN, 471 MHz, 298K) δ[ppm] =-70.35 (d, *J* = 714.7 Hz), -72.54 (d, *J* = 707.8 Hz).

MS (ESI-MS, positive mode): m/z $[Fe_4L_6(PF_6)_5]^{3+}$ (calcd. 1409.16): found 1409.16, $[Fe_4L_6(PF_6)_4]^{4+}$ (calcd. 1020.63): found 1020.56, $[Fe_4L_6(PF_6)_3]^{5+}$ (calcd. 787.51): found

787.40, $[Fe_4L_6(PF_6)_2]^{6+}$ (calcd. 632.10): found 631.95, $[Fe_4L_6(PF_6)]^{7+}$ (calcd. 521.10): found 437.83

Alternatively, the cage can be assembled through the exact same experimental procedure, substituting $Fe(PF_6)_2$ for $Fe(OTf)_2$; however, the resulting ^{1}H NMR spectrum of this assembly

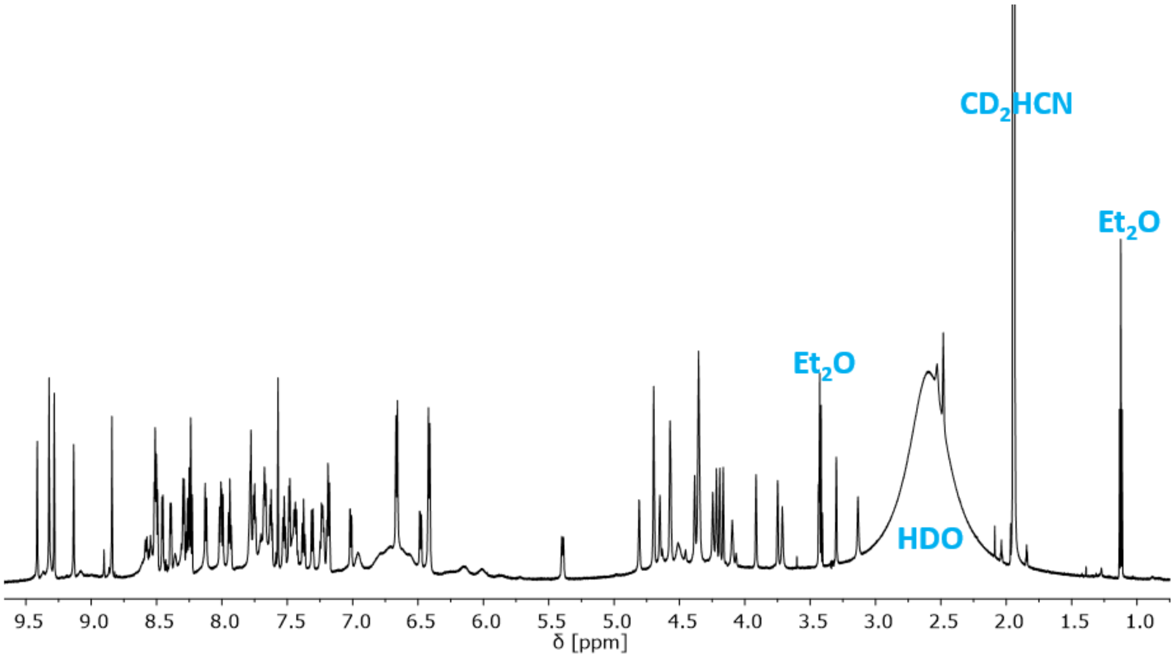

Figure S1: ^{1}H NMR Spectrum (CD_3CN, 700 MHz, 298K) of **1(PF$_6$)$_8$**.

Assignment comments: Imine protons were identified by ^{1}H-^{13}C HSQC and the absence of coupling. From there, H-4 was identified by ^{1}H-^{13}C HMBC and ^{1}H-^{1}H NOESY spectra. The rest of the pyridine moiety was assigned through ^{1}H-^{1}H COSY correlations. Assignment of the phenylene protons is not possible due to broadening and overlap; hence, correlation between the pyridylimine and ferrocene region was not possible. However, 6-fold dessymetrization can be seen in both regions. At lower temperature (238 K), we could resolve the broad phenylene protons into distinct, individual signals.

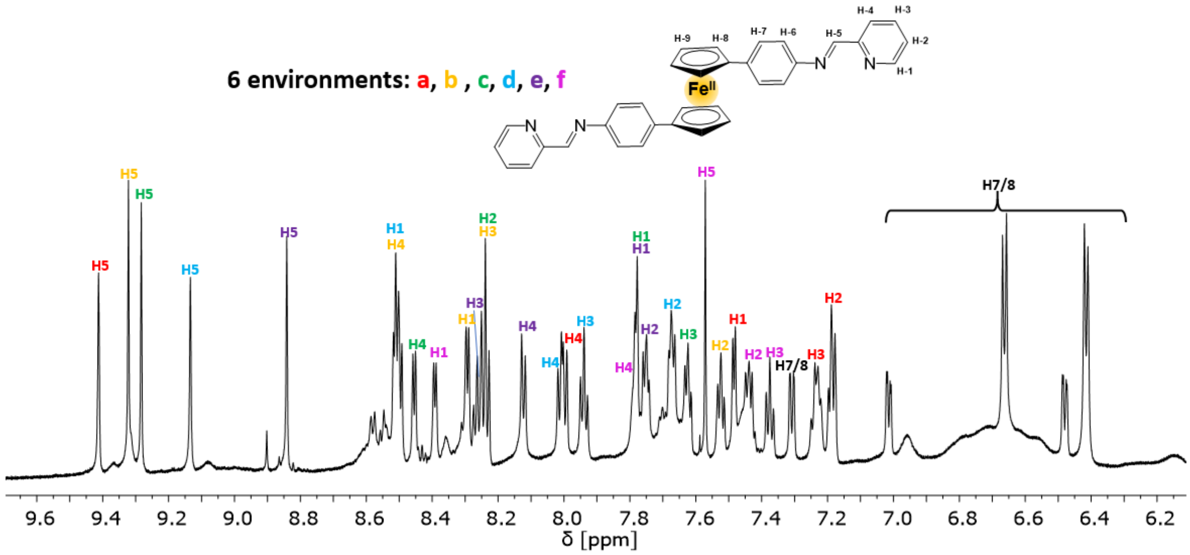

Figure S2: Aromatic region of the ^{1}H NMR spectrum (CD_3CN, 700 MHz, 298 K) of **1**.

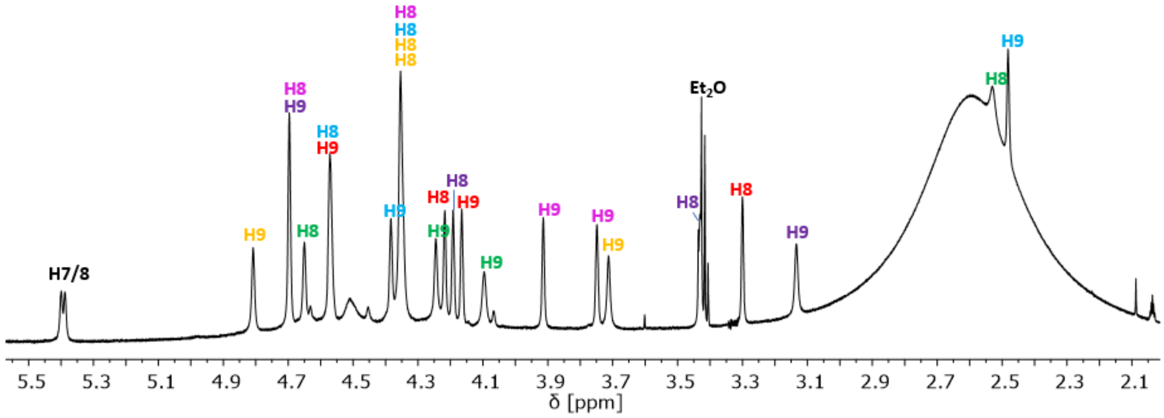

Figure S3: Ferrocene region of the ^{1}H NMR spectrum (CD_3CN, 700 MHz, 298 K) of **1**.

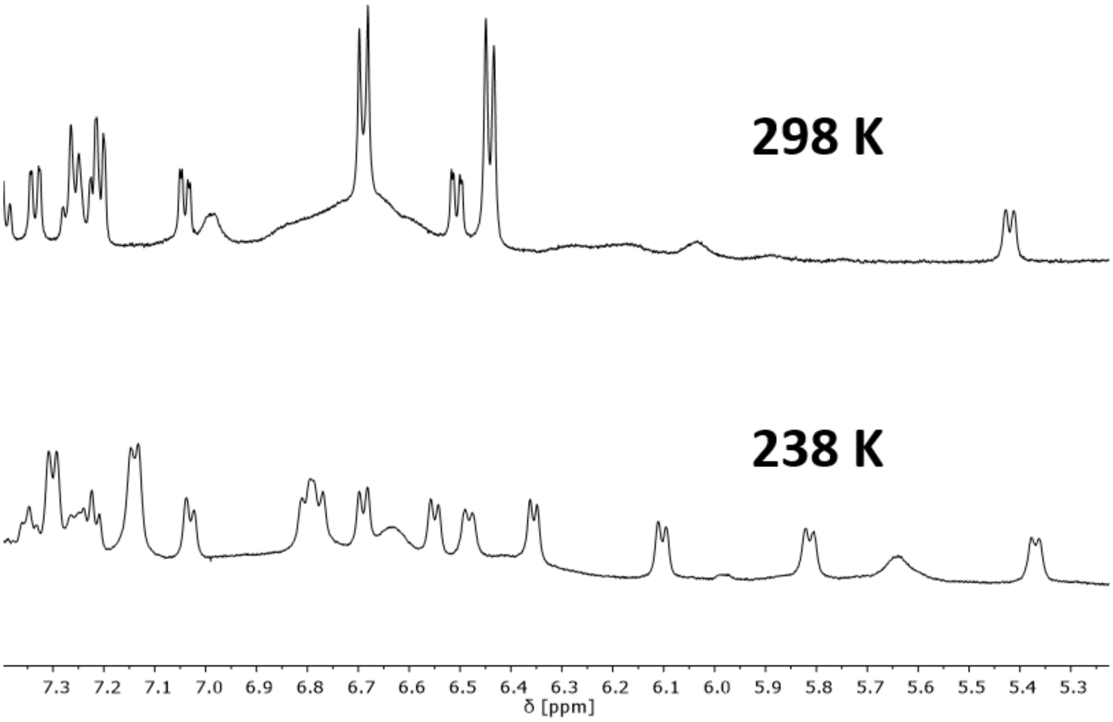

Figure S4: Phenylene region of the ^{1}H NMR spectrum (CD_3CN, 500 MHz) of **1** at 238 K and 298 K showing sharpening of the phenylene resonances upon cooling.

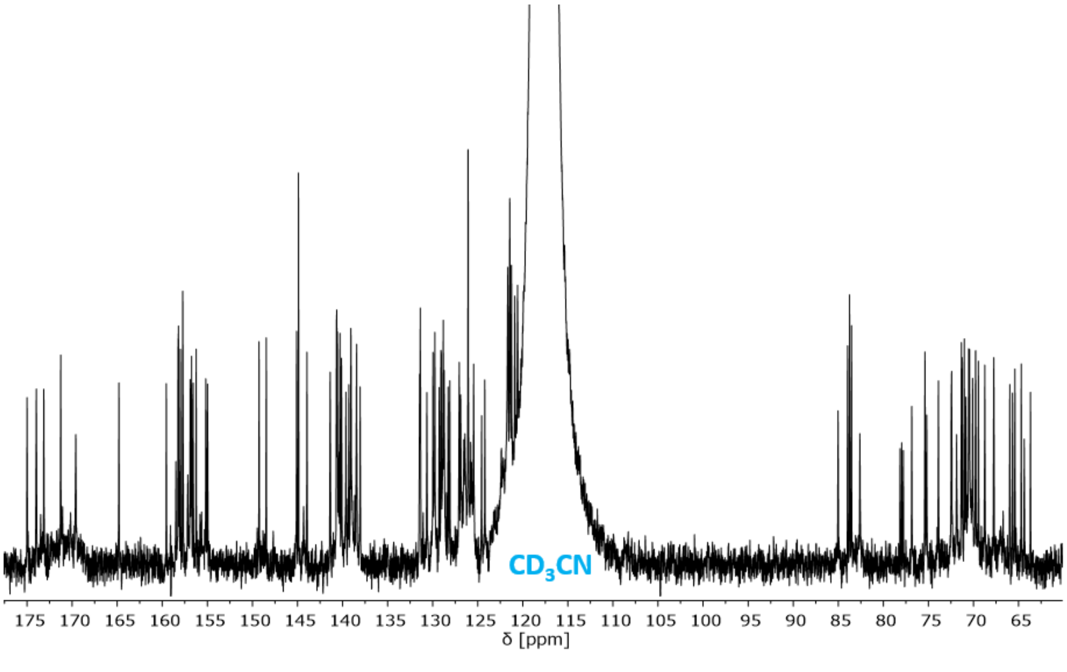

Figure S5: ^{13}C NMR spectrum (CD_3CN, 176 MHz, 298 K) of **1**.

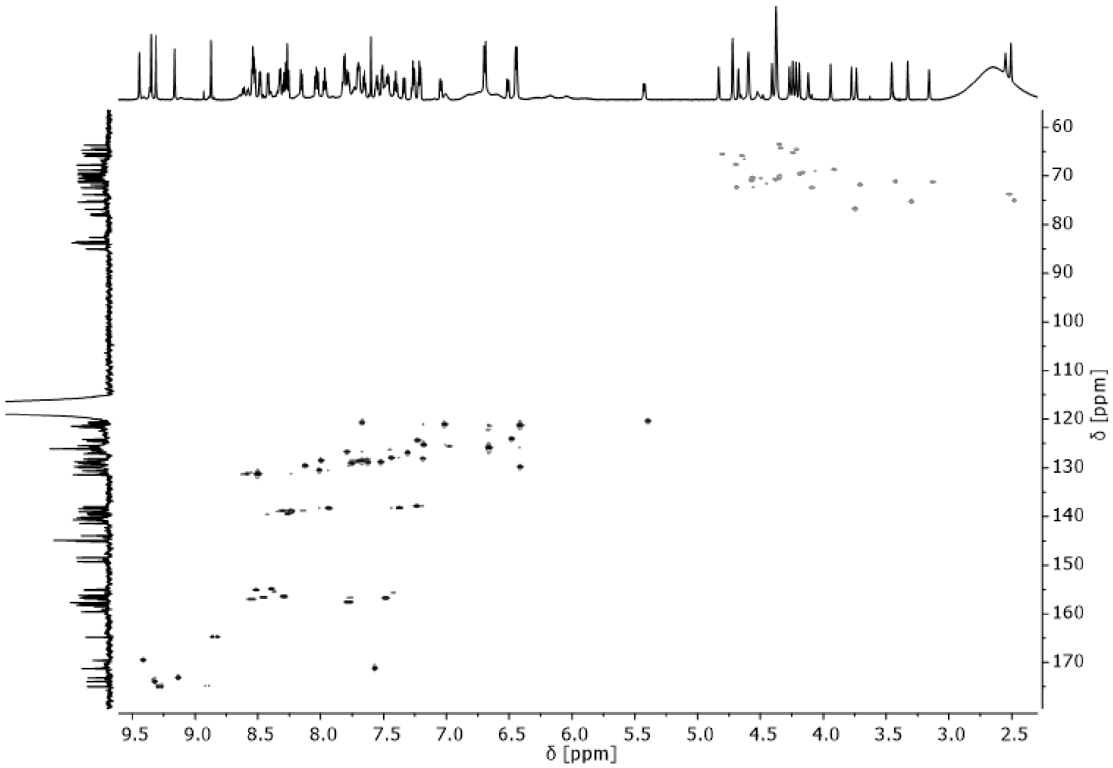

Figure S6: ^{1}H-^{13}C HSQC NMR spectrum (CD_3CN, 176 MHz, 298K) of **1**.

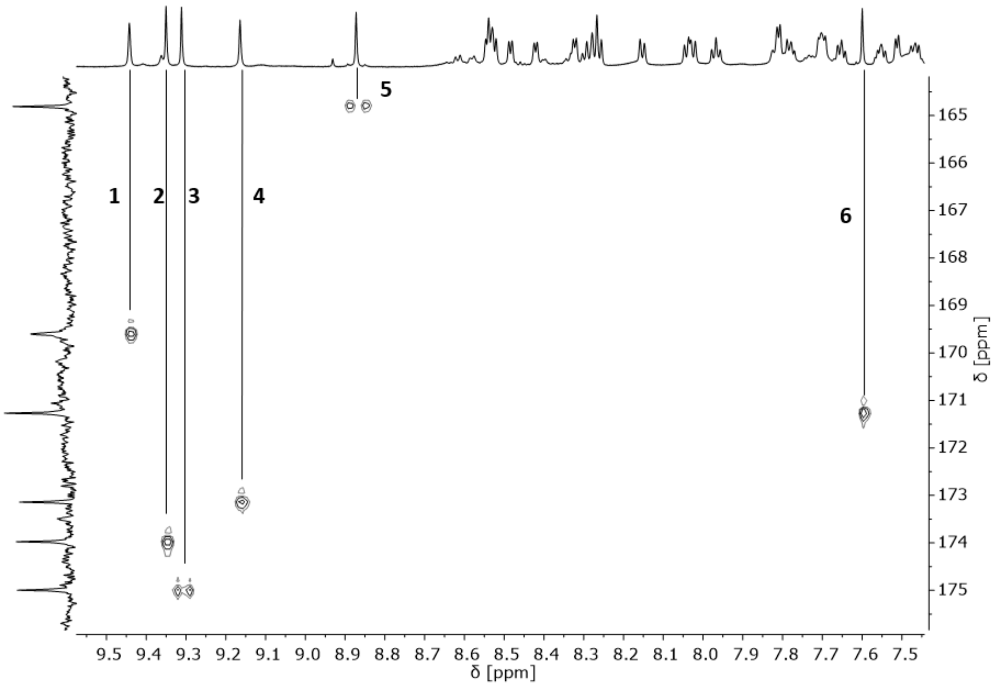

Figure S7: Partial ^{1}H-^{13}C HSQC NMR spectrum (CD_3CN, 176 MHz, 298K) of **1** highlighting the 6 imine resonances resulting from 2 meridional coordination environments.

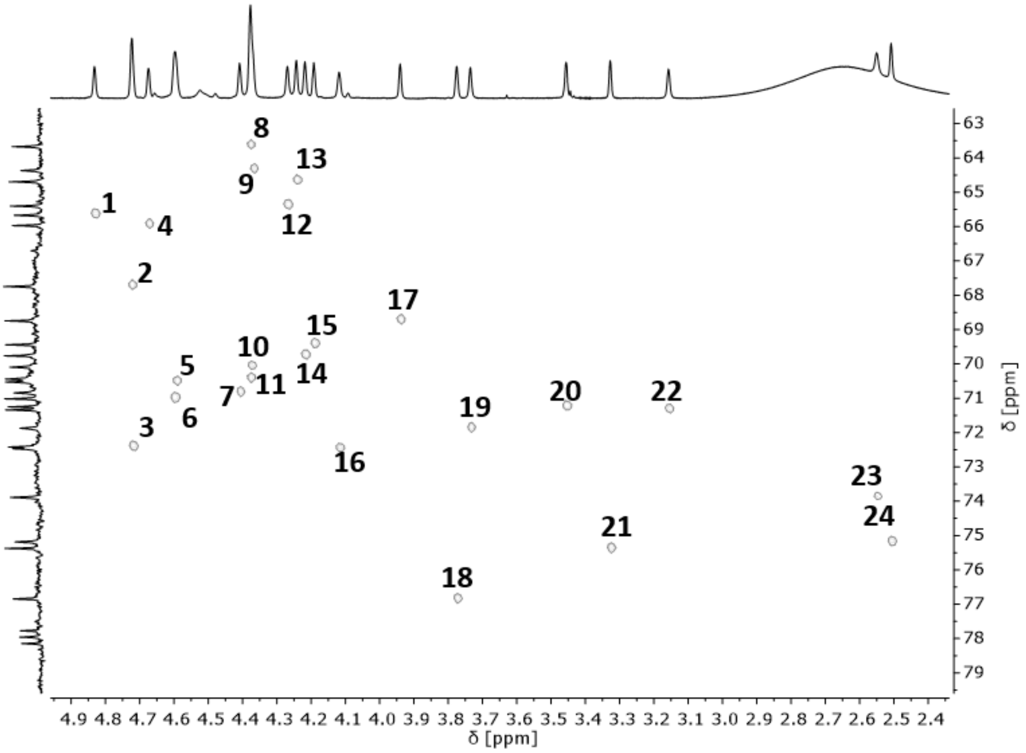

Figure S8: Partial ^{1}H-^{13}C HSQC NMR spectrum (CD$_3$CN,176 MHz, 298K) of **1** highlighting the 24 CH ferrocene resonances resulting the restricted axial rotation in **1**. 6 coordination environments and 4 ferrocene protons per linker gives 24 resonances.

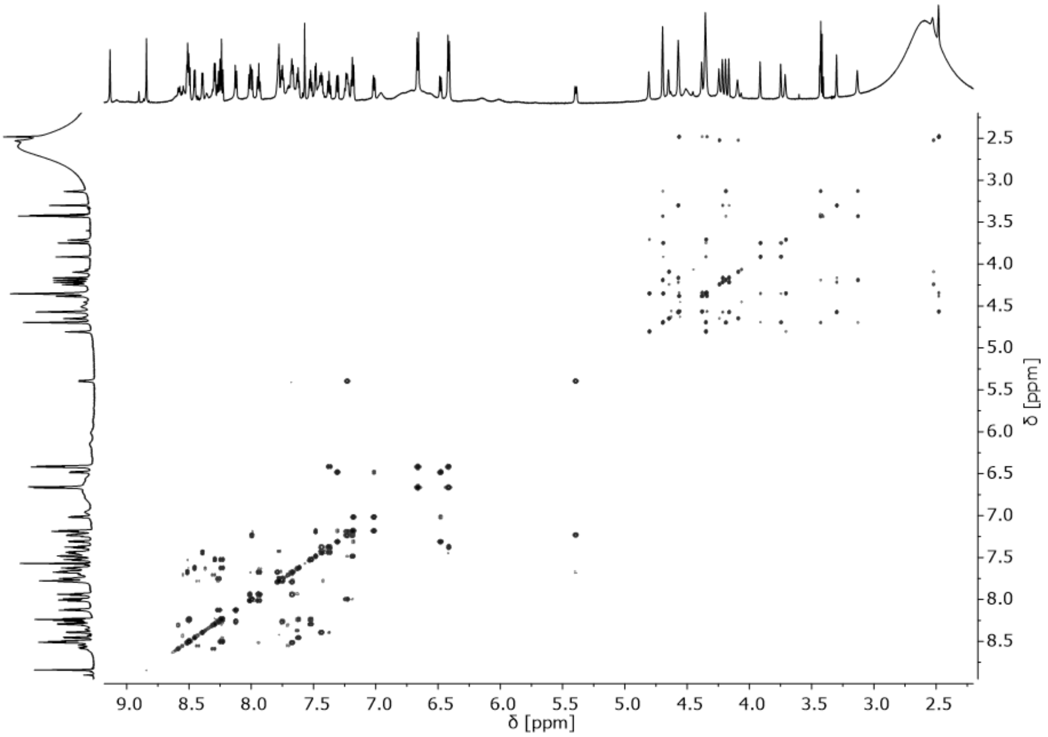

Figure S9: ^{1}H-^{1}H COSY NMR spectrum (CD$_3$CN, 700 MHz, 298 K) of **1**.

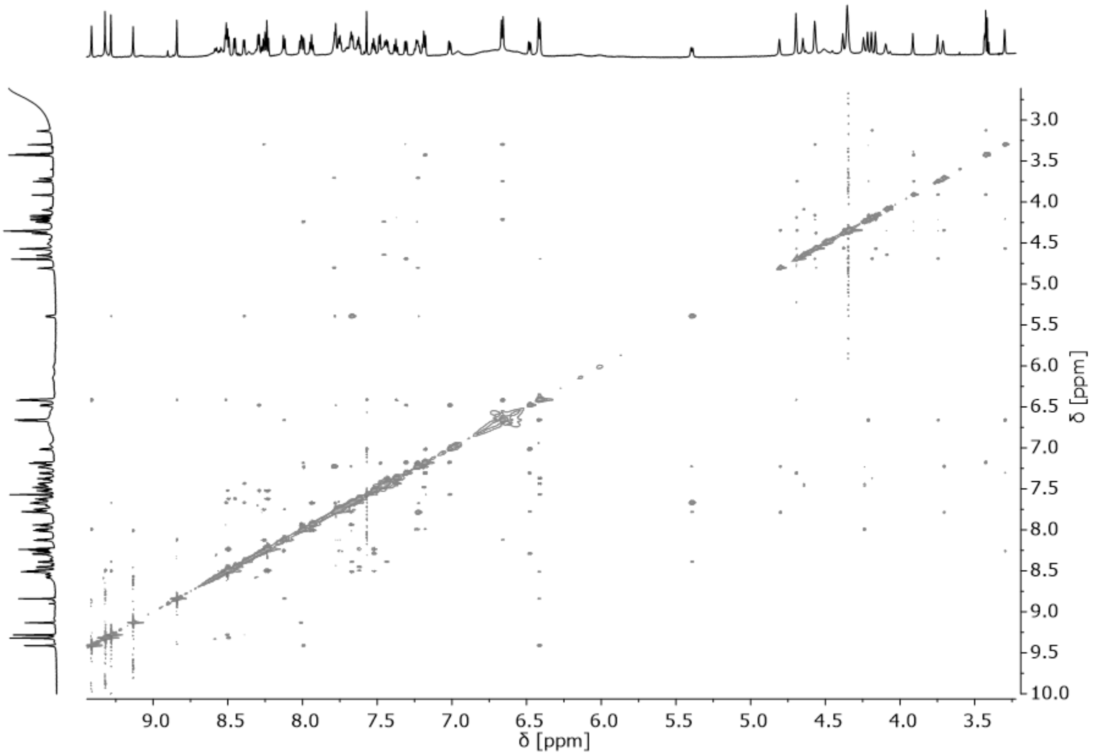

Figure S10: ^{1}H-^{1}H NOESY NMR spectrum (CD_3CN, 700 MHz, 298 K) of **1**.

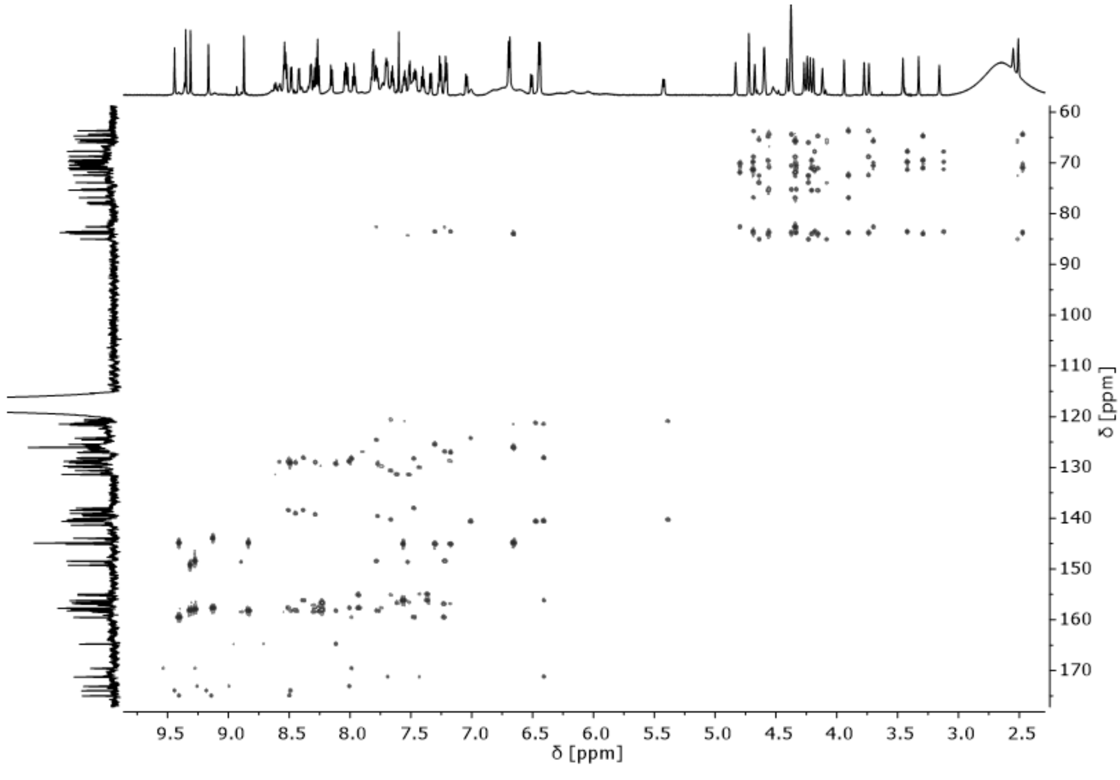

Figure S11: ^{1}H-^{13}C HMBC NMR spectrum (CD_3CN, 176 MHz, 298 K) of **1**.

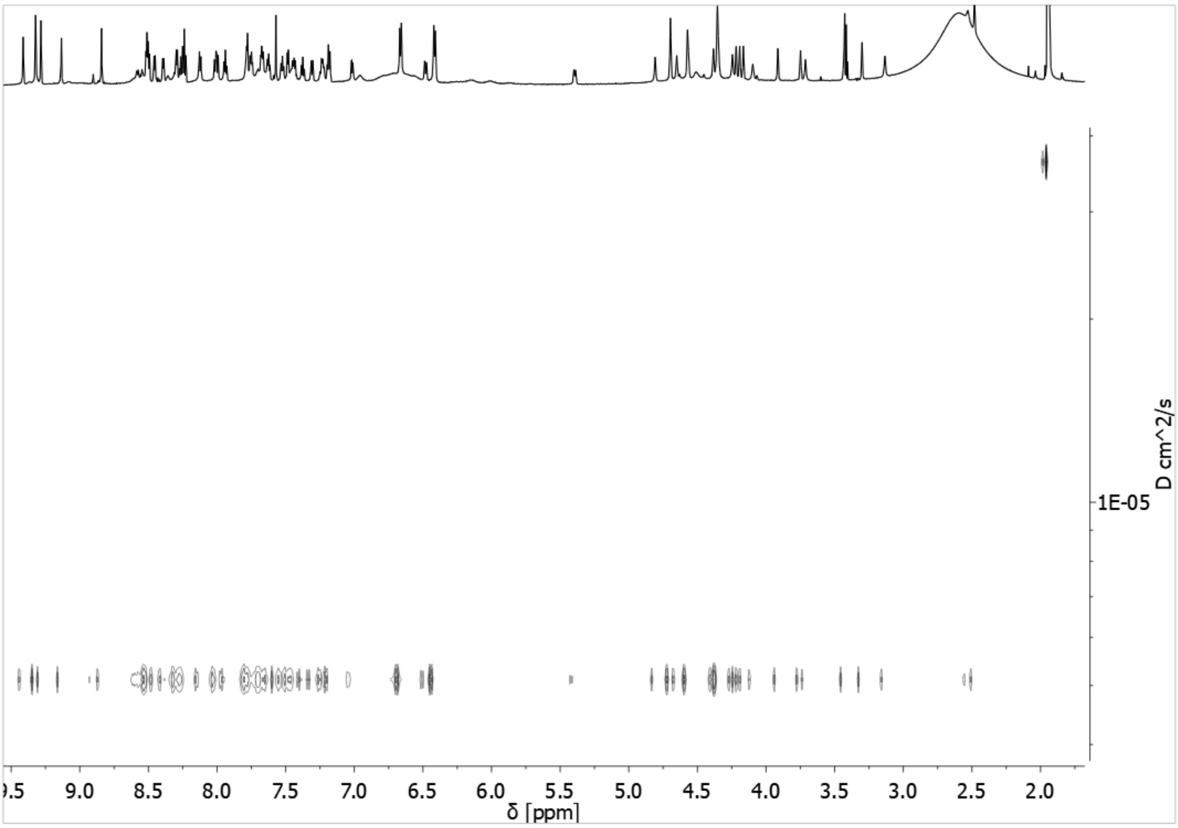

Figure S12: ^{1}H DOSY NMR spectrum (400 MHz, CD_3CN, 298 K) of **1**.

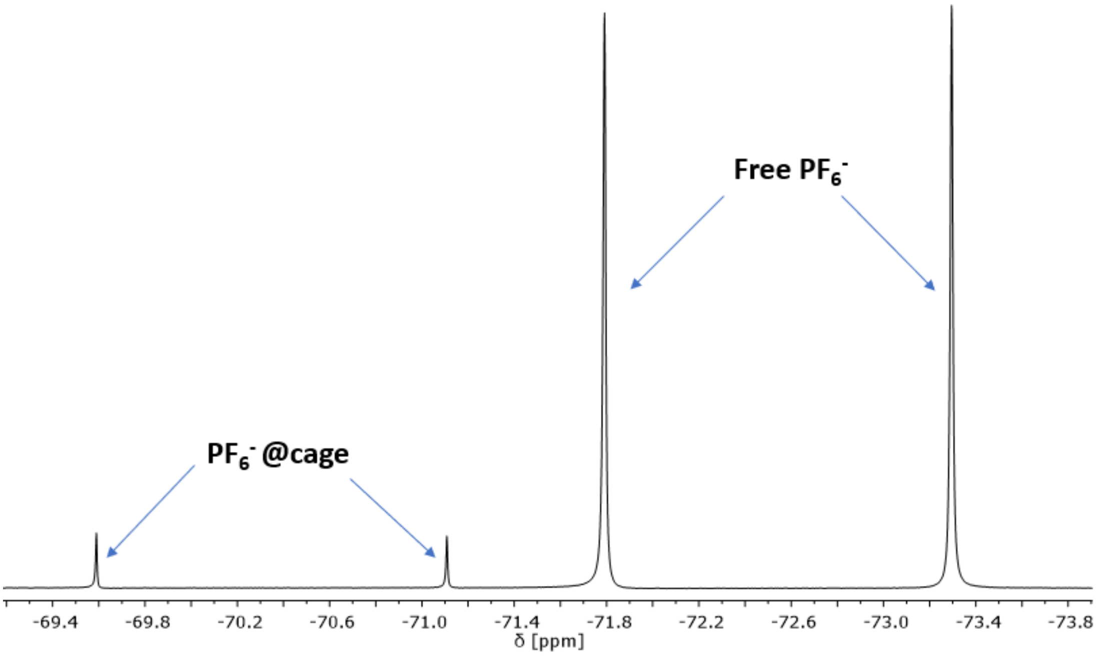

Figure S13: ^{19}F NMR (470 MHz, CD_3CN, 298 K) spectrum of **1**.

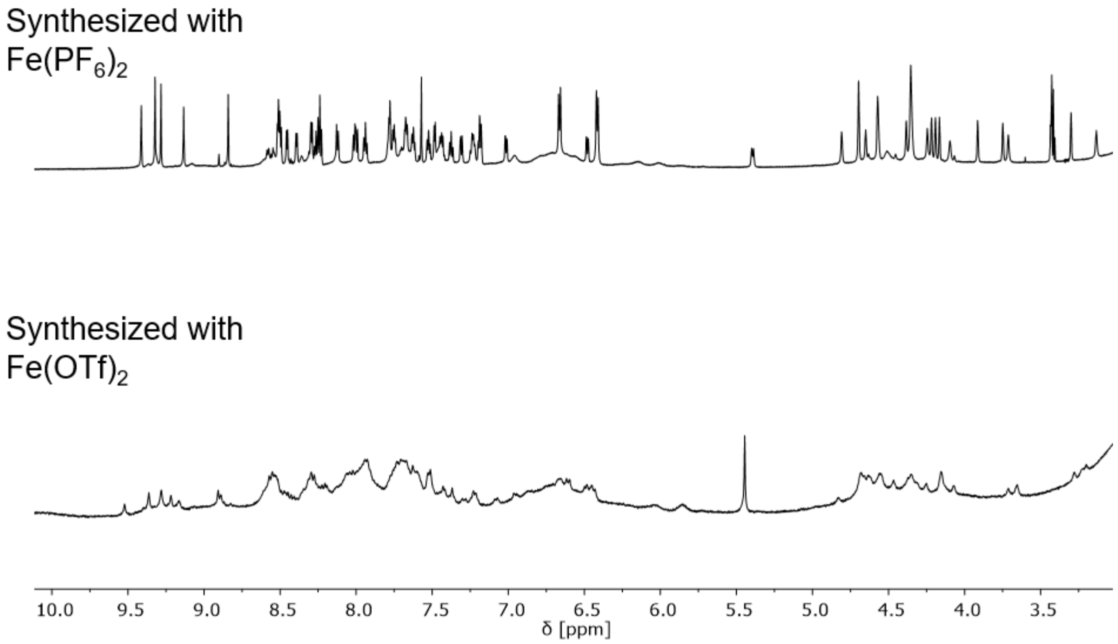

Figure S14: Comparison between the ^{1}H NMR spectrum (CD_3CN, 700 MHz top, 400 MHz bottom, 298K) of the PF_6^- and OTf^- salt of **1**; singlet at 5.5 corresponds to residual DCM from the ligand.

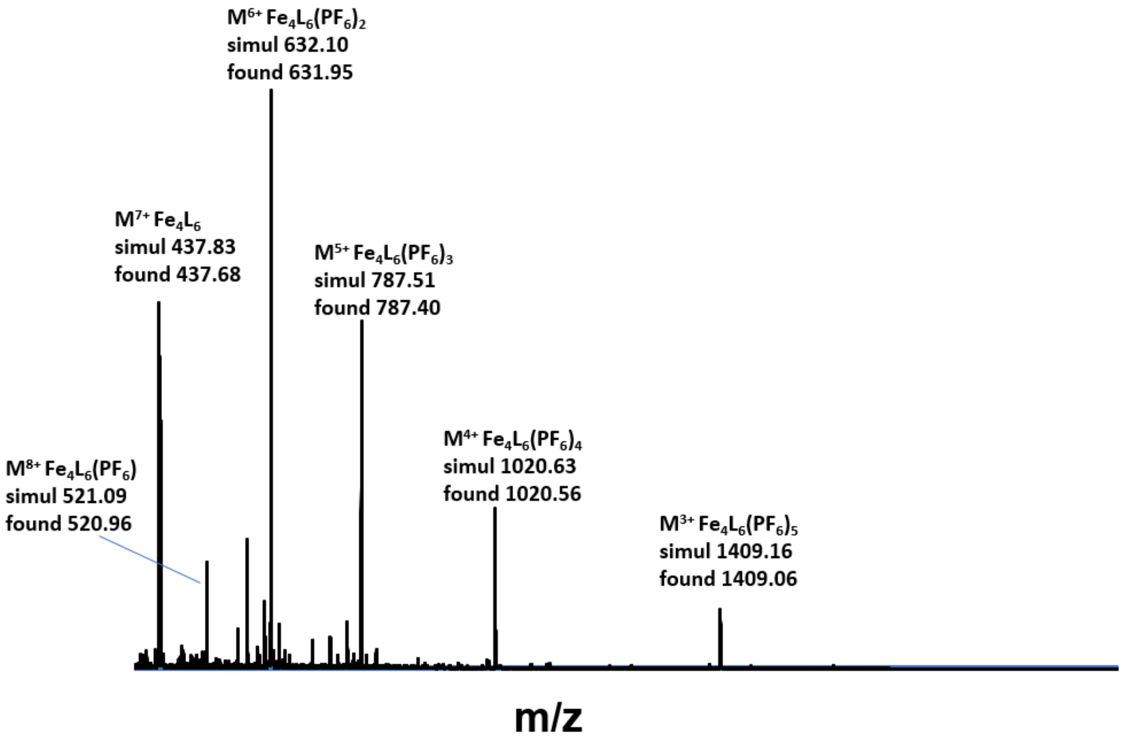

Figure S15: Low resolution ESI mass spectrum of **1** in CH_3CN.

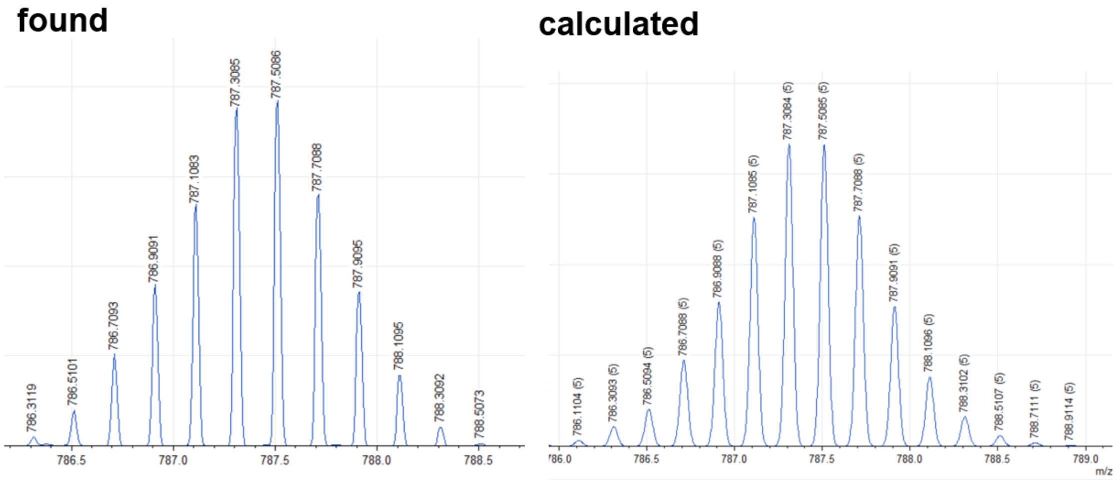

Figure S16: High resolution ESI mass spectrum (positive mode) in CH_3CN; zoom in on M^{5+} peak of **1** in CH_3CN and calculated isotope pattern for M^{5+} peak ion of **1** in CH_3CN.

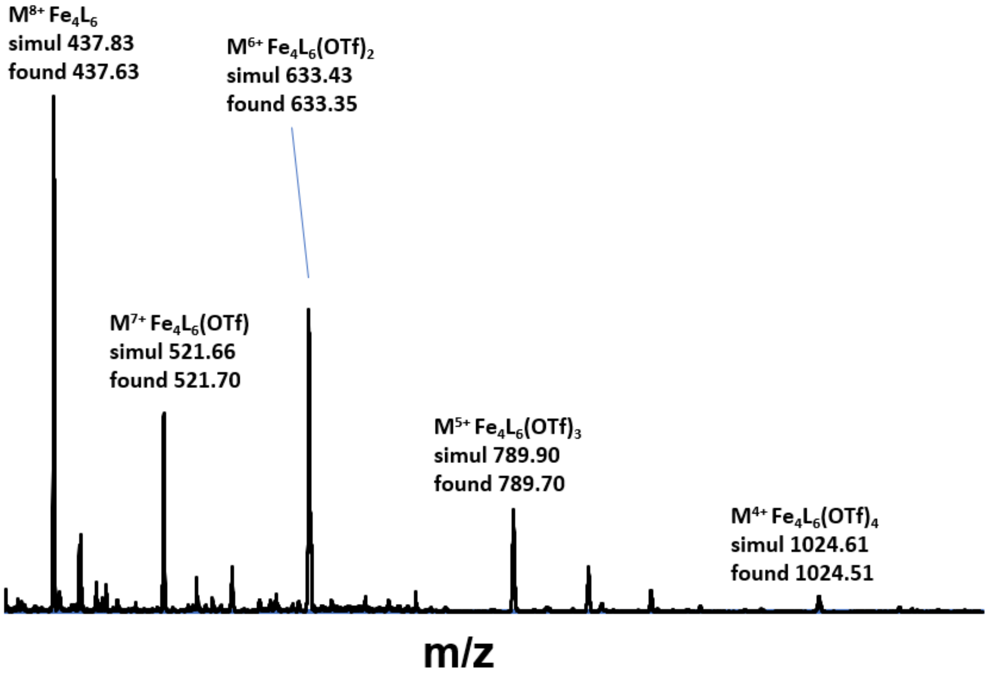

Figure S17: Low resolution ESI mass spectrum (positive mode) derivative of **1** assembled from **A**, 2-pyridinecarboxaldehyde and $Fe(OTf)_2$ in CH_3CN.

2.1 Cyclic Voltammetry of 1

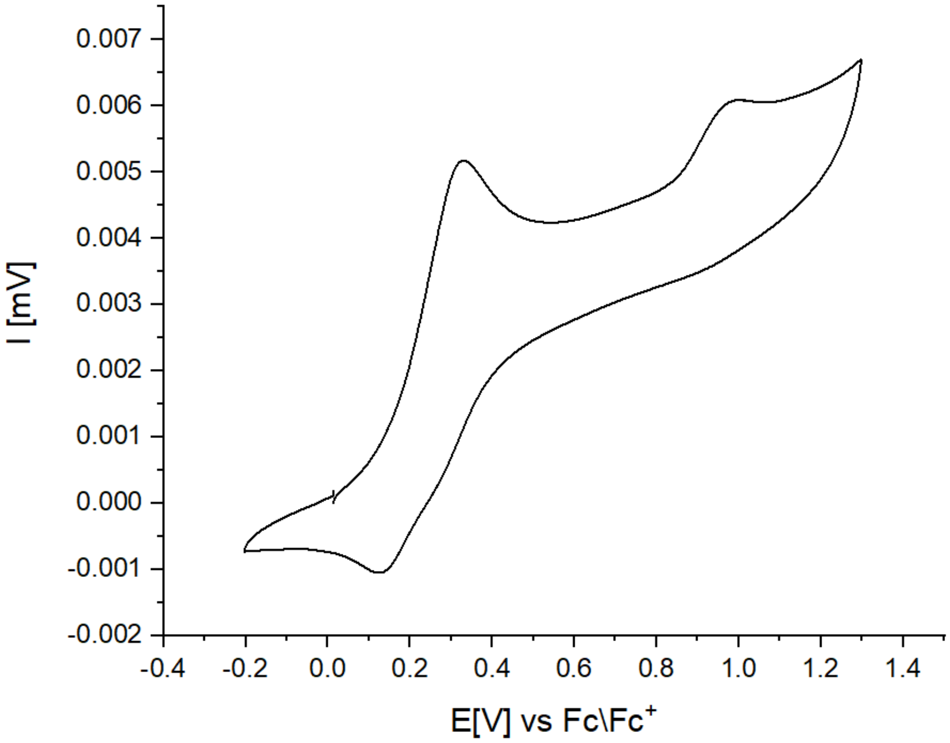

Figure S18: CV of **1** in 0.1 M nBu_4NPF_6/CH_3CN electrolyte at a scan rate of 10 mV/s.

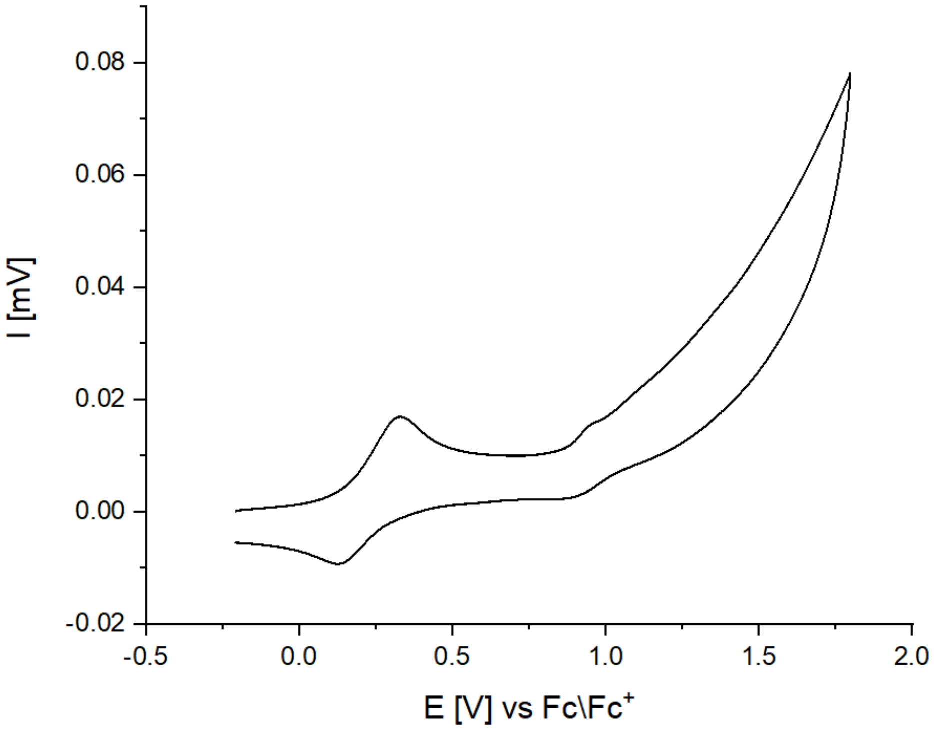

Figure S19: CV of **1** in 0.1 M nBu_4NPF_6/CH_3CN electrolyte at a scan rate of 100 mV/s.

2.2 Synthesis and assembly of 1-1'-Bis(4-(2-pyridyldiazenyl)phenyl)ferrocene (L^{azo})

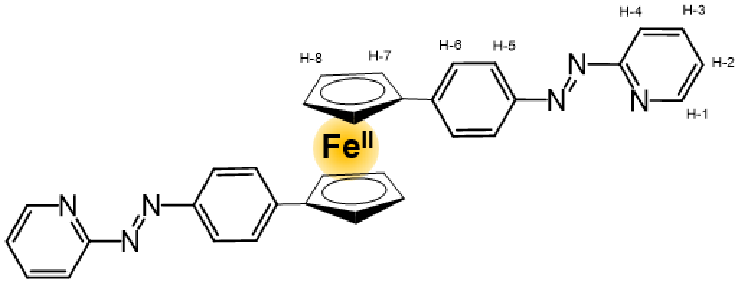

1-1'-Bis(4-aminophenyl)ferrocene (100 mg, 0.27 mmol) and 2-nitrosopyridine (59 mg, 0.54 mmol) were dissolved in CH_2Cl_2 (5 mL). Glacial AcOH (1 ml) was added, and the solution was stirred at room temperature for 16 hours. The mixture was neutralised with saturated sodium bicarbonate and diluted with 10 ml of CH_2Cl_2. The organic phase was separated and washed with brine, water and dried over magnesium sulfate. The solvent was removed and the crude product suspended in boiling water and isolated by filtration. Yield $\mathbf{L^{azo}}$ (76%, 0.205mmol).

^{1}H NMR ($CDCl_3$, 400 MHz, 298K): δ[ppm] = 8.70 (d, *J* = 3.9 Hz, 2H), 7.84 (d, *J* = 8.5 Hz, 4H), 7.82 – 7.75 (m, 2H), 7.72 (d, *J* = 7.9 Hz, 2H), 7.35 (d, *J* = 8.4 Hz, 6H), 4.65 (s, 4H), 4.39 (s, 4H). See figure below for assignment.

^{13}C NMR ($CDCl_3$,101 MHz, 298K): δ[ppm] = 163.11, 150.50, 149.38 , 142.43 , 138.09 , 126.15 , 124.70 , 123.89 , 115.17 , 84.84 , 71.30 , 68.27.

HRMS (ESI-MS, positive mode): m/z $[M+H]^+$ (calcd. 549.1490) found 549.1510.

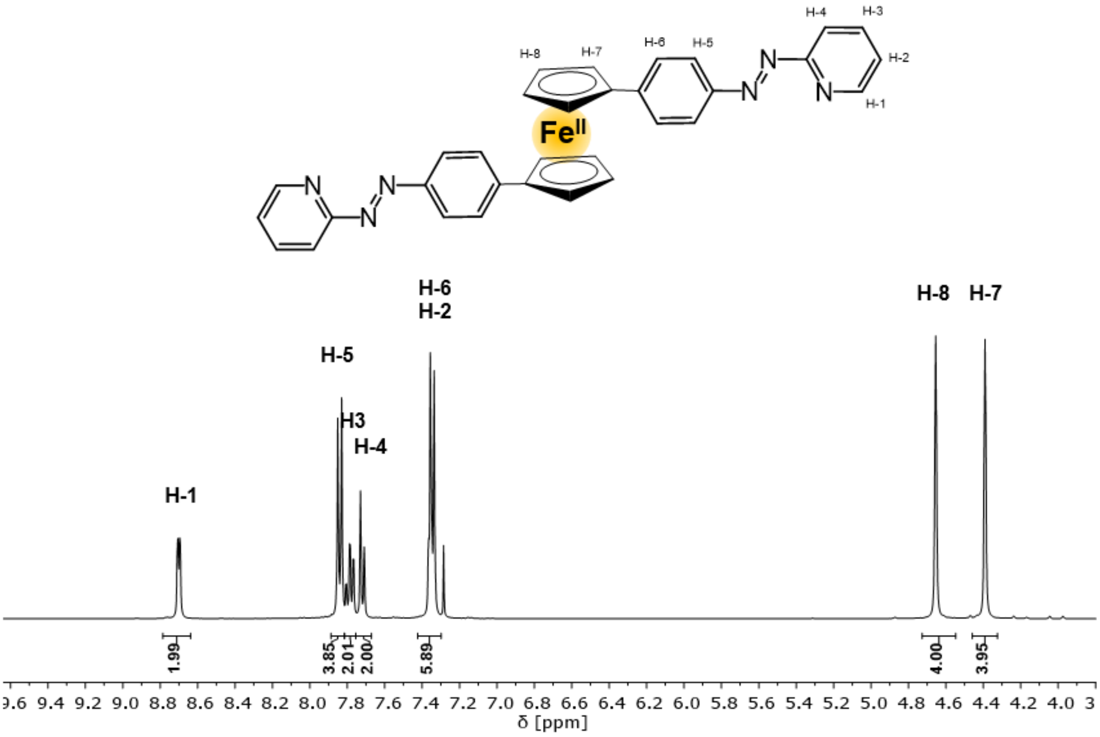

Figure S20: ^{1}H NMR spectrum ($CDCl_3$, 400 MHz, 298K) of **L^{azo}**.

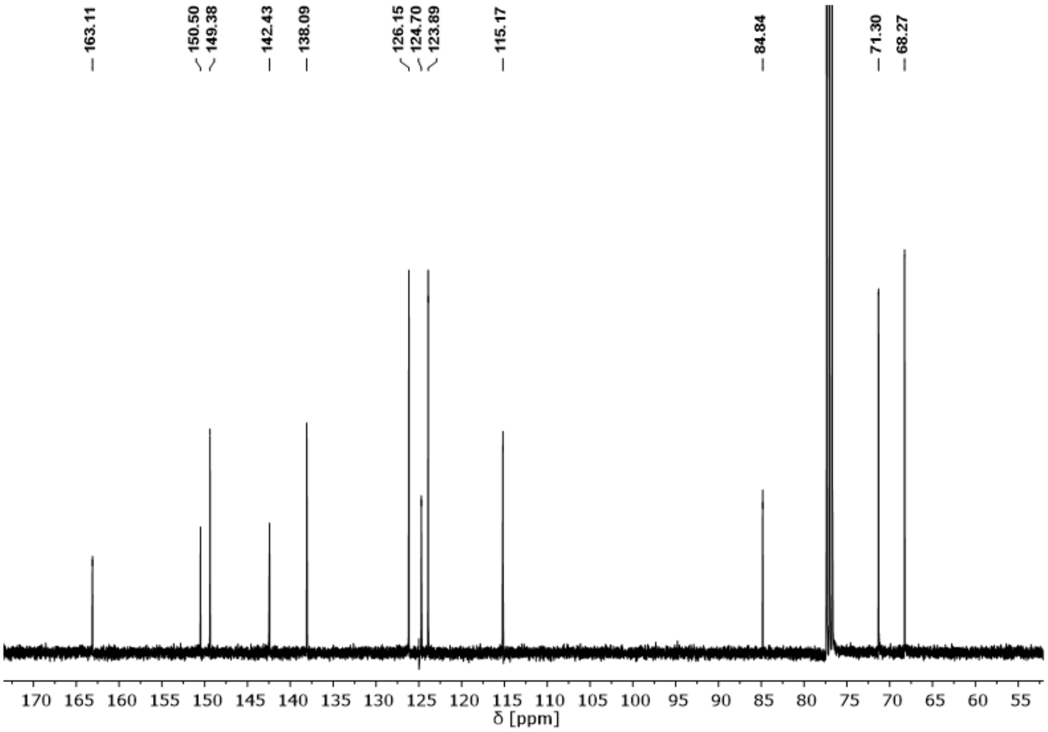

Figure S21: ^{13}C NMR spectrum ($CDCl_3$,101 MHz, 298K) of **L^{azo}**.

Employing the pre-formed ligand **B** (in place of **A** and 2-pyridylcarboxaldehyde) with $Fe(NTf_2)_2$ likewise produced a Fe_4L_6 congener of **1** by ESI-MS; however, the ^{1}H NMR signals of this derivative were likewise too broad to allow full NMR characterization.

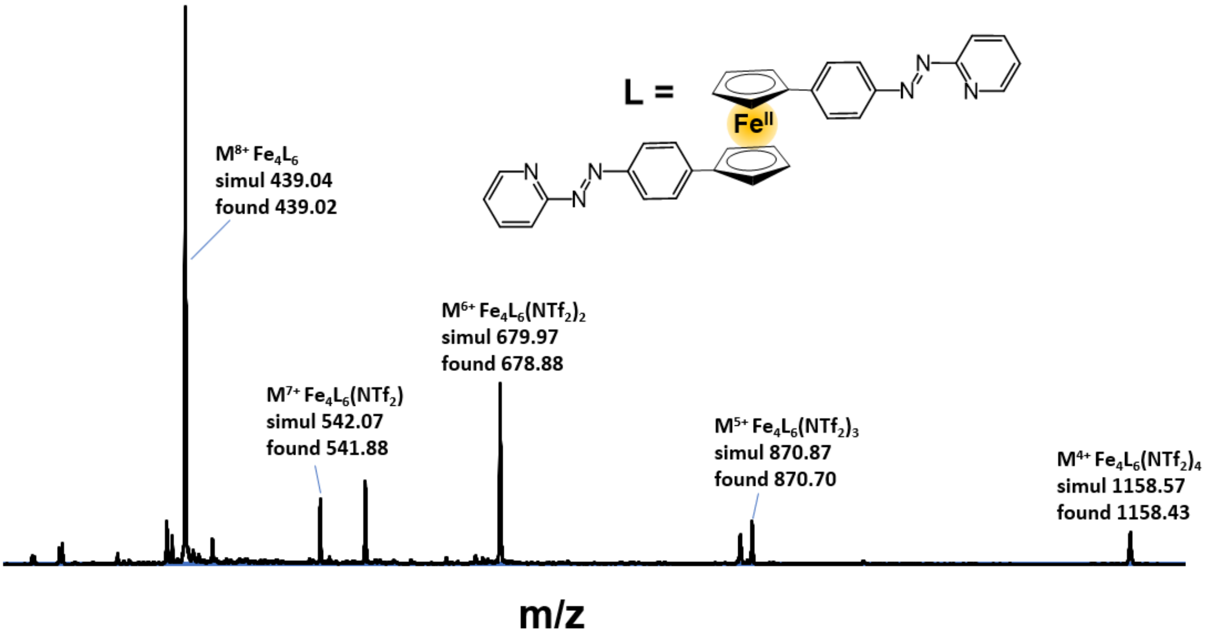

Figure S22: Low resolution ESI mass spectrum (positive mode) the derivative in of **1** assembled from $\mathbf{L^{azo}}$ and $Fe(NTf)_2$ in CH_3CN.

3. Oxidative disassembly into mononuclear complexes

To a solution of **1** (5.0 mg, 1.1 µmol) in 1 ml of CH_3CN was added $NOPF_6$ (1.2 mg, 6.6 µmol) in 0.5 ml inside a N_2 filled glovebox. The resulting orange solution was filtered using a syringe filter and transferred to a J. Young tube and connected to a Schlenk line. 7 ml of Et_2O were added precipitate **1.** The supernatant was syringed from the flask and the solid product was washed with H_2O and THF and dried *in vacuo* to yield **2** as an orange powder (3.9 mg, 3.8 µmol, 86%).

The yield is given considering that **1** only provides 4 Fe(II) per 6 ligands. Thus, only 4 mononuclear complexes **2** can be generated from one equivalent of **1**.

^{1}H NMR (400 MHz, CD_3CN, 298K) δ[ppm]= 144.84, 90.85, 58.90, 57.60, 53.20, 45.99, 35.64, 31.88,16.85, -10.70, -21.74.

^{19}F NMR (376 MHz, CD_3CN, 298K) δ[ppm]= -74.07 (d, J = 706.5 Hz).

MS (ESI-MS): m/z $(FeL^{(+)}(PF6)_2)^+$ (calc 899.01) found 892.12; $(FeL^{(+)}PF_6)^{2+}$ calc (373.52) found 373.40; $(FeL^{(+)})^{3+}$ (calc 200.69) found 200.57

MS (HRESI-MS): m/z $FeL(CH_3CN)^{3+}$ (calc 214.3072) 214.3695**.**

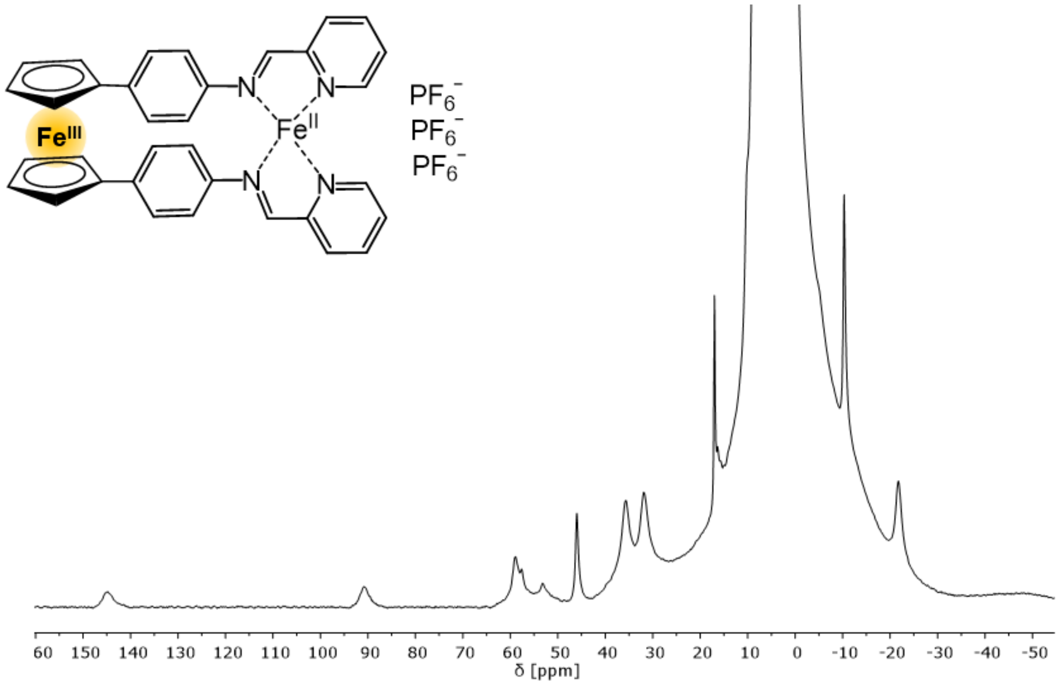

Figure S23: Wide sweep ^{1}H NMR spectrum (CD_3CN, 400 MHz, 298 K) of **2**.

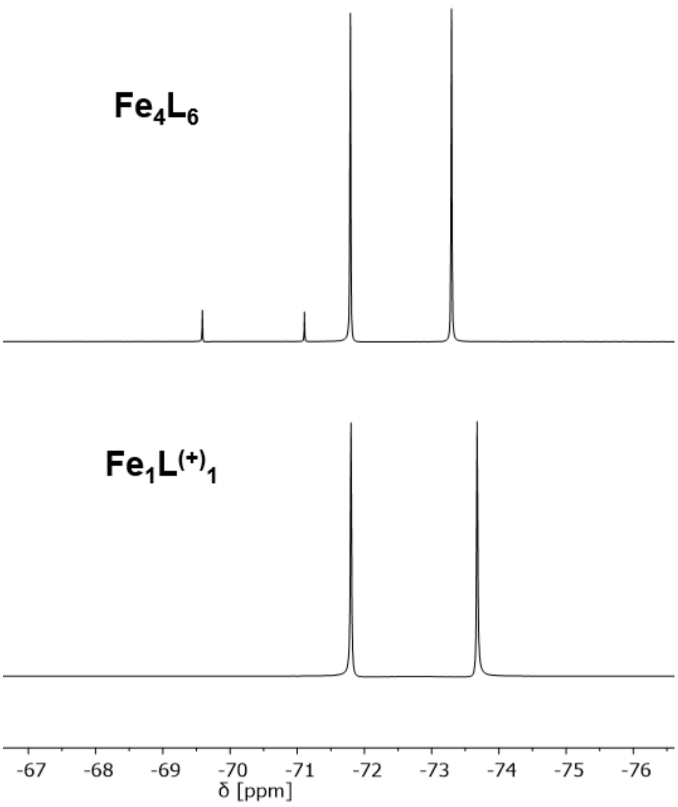

Figure S24: ^{19}F NMR spectrum (CD_3CN, 376.3 MHz, 298K) of **2;** signals stacked for clarity.

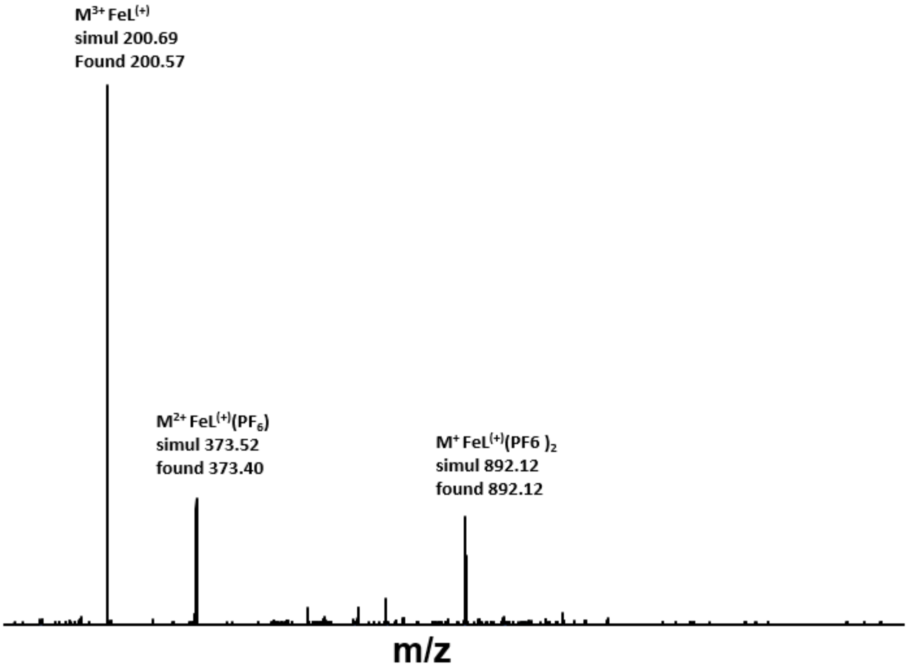

Figure S25: LR-ESI-MS (positive mode) of the mononuclear **2** complex in MeOH.

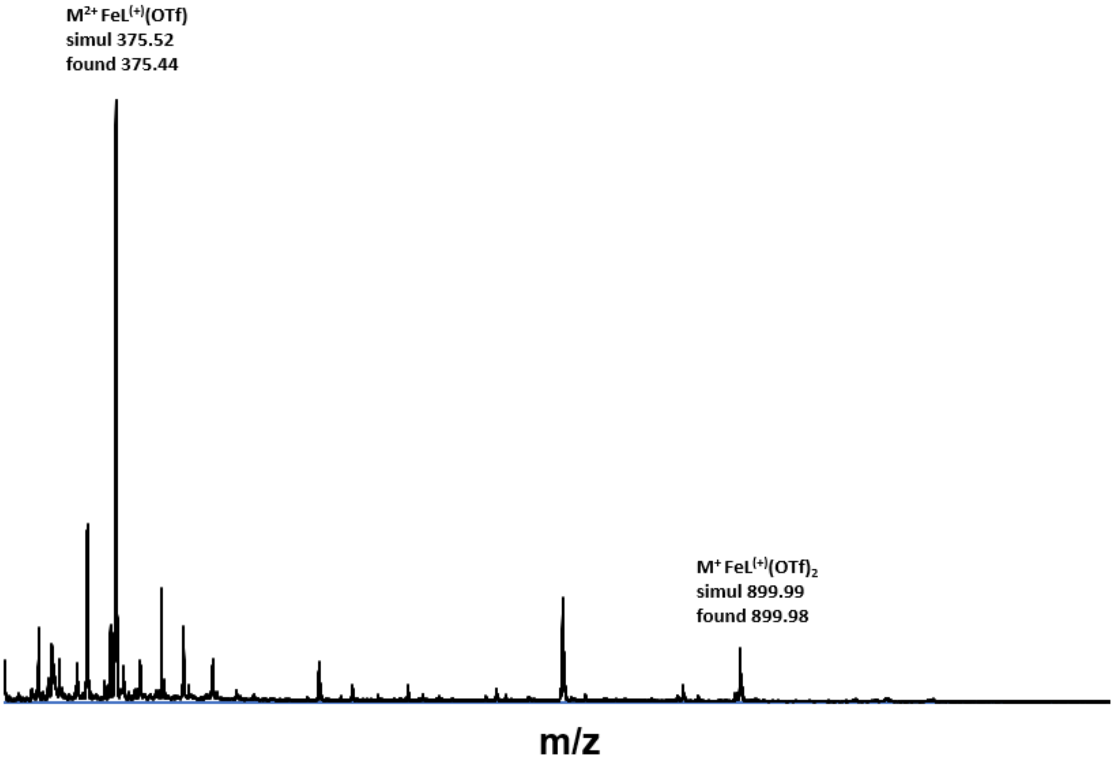

Figure S26: LR-ESI-MS (positive mode) of the mononuclear complex **2** generated from the OTf$^-$ salt of **1** in MeOH.

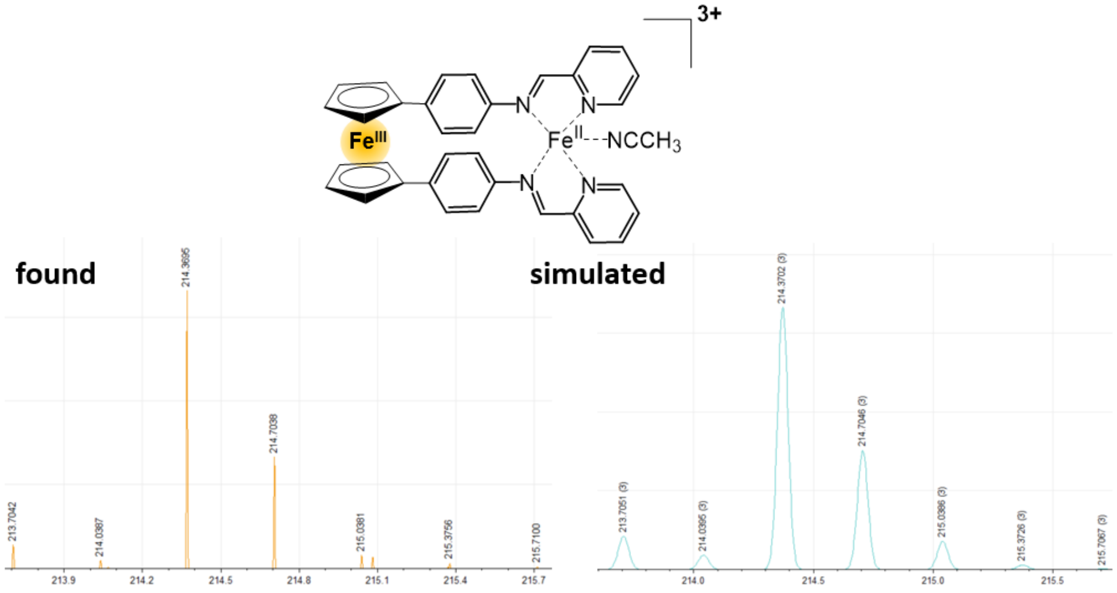

Figure S27: HR-ESI-MS of the +3 peak of the acetonitrile adduct of **2** in CH_3CN, indicating acetonitrile coordination in solution.

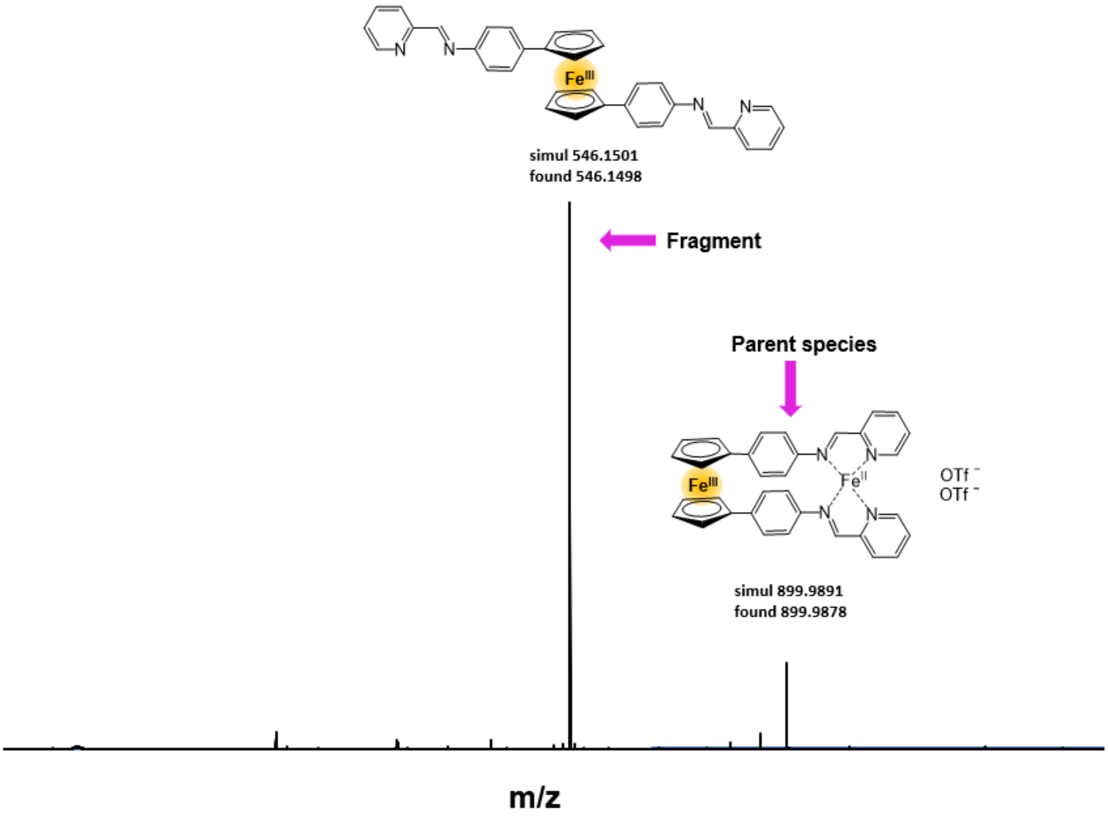

Figure S28: HR-ESI-MS/MS of **2**(OTf)$_2$ showing fragmentation of the mononuclear complex in CH$_3$CN into the oxidized ligand, showing that oxidation is occurring at the ferrocene unit. No presence of protonated Fe^{II}-ferrocene species was observed.

4. Investigations of the transformation of 1 into 2

4.1 NMR Titration

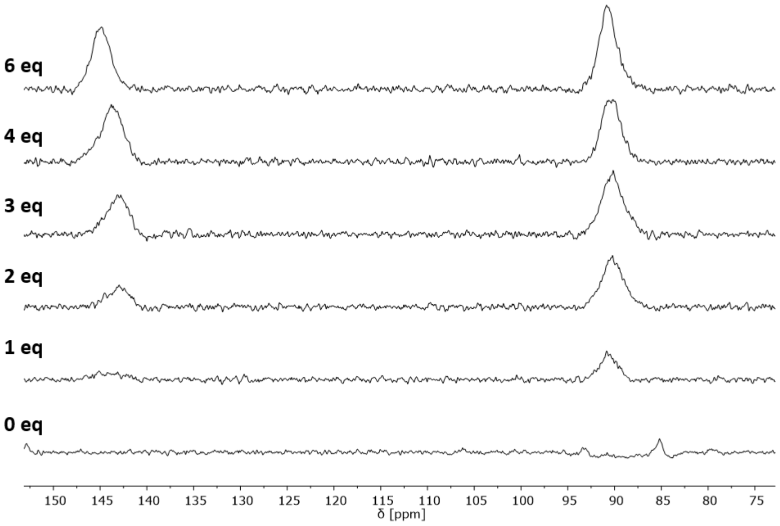

Figure S29: Partial wide-sweep ^{1}H NMR spectrum of the titration of **1** with $NOPF_6$ in CD_3CN showing the gradual increase of the mononuclear species upon cage oxidation.

4.2 Spectroelectrochemistry and optical titrations

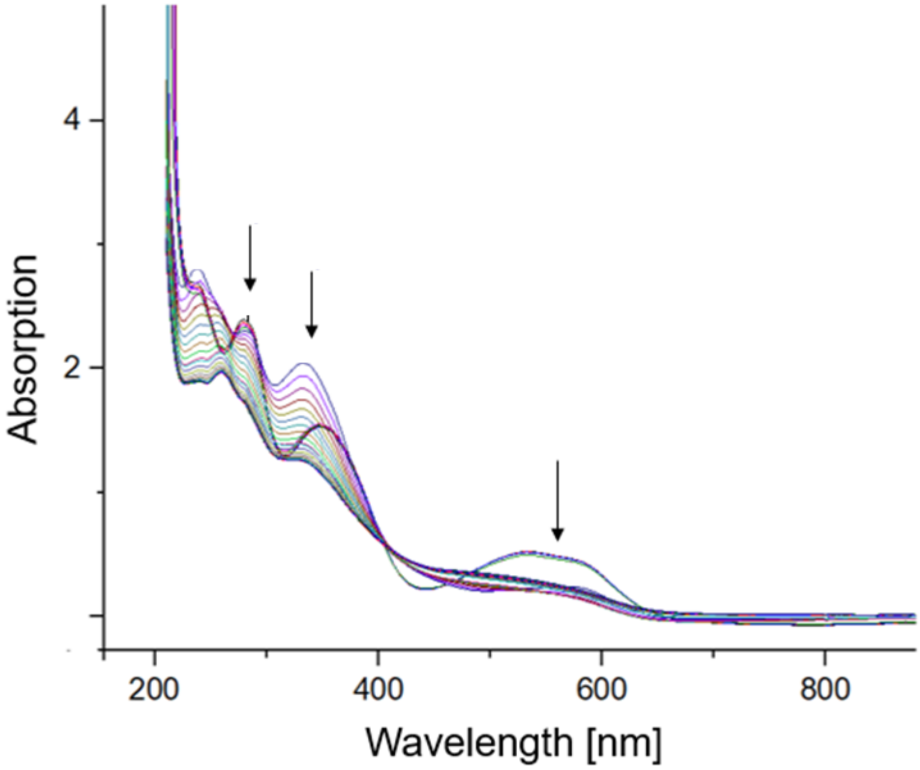

Figure S30: UV-Vis spectroelectrochemistry of **1** (3 µM in CH_3CN) in 0.3 M $nBuNPF_6/CH_3CN$ electrolyte upon oxidation at +0.7 V vs. Ag^+/Ag (quasi-reference).

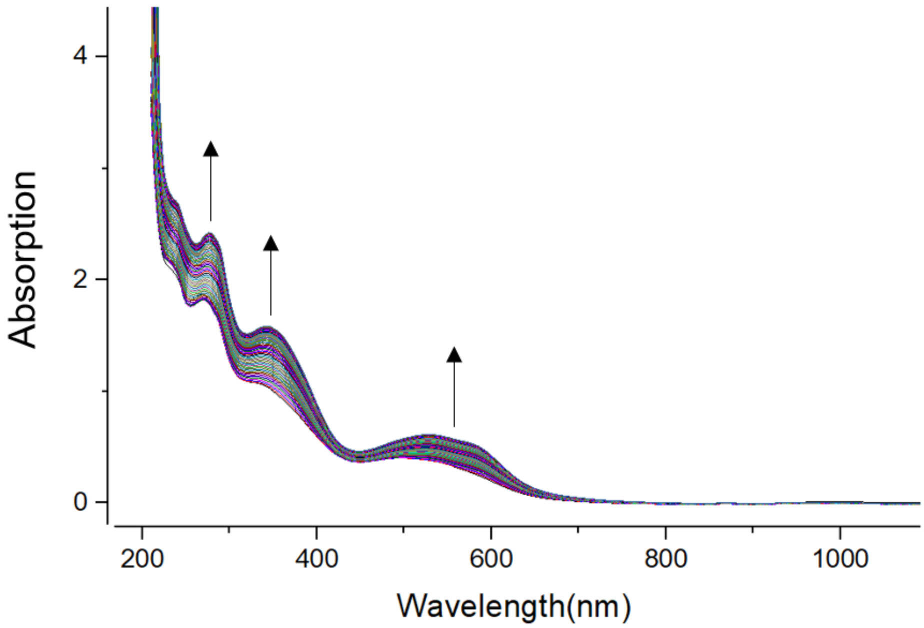

Figure S31: UV-Vis spectroelectrochemistry of **1** (3µM in CH_3CN) in 0.3 M $nBuNPF_6/CH_3CN$ electrolyte, following spectral changes at 0 V vs. Ag^+/Ag, after oxidation.

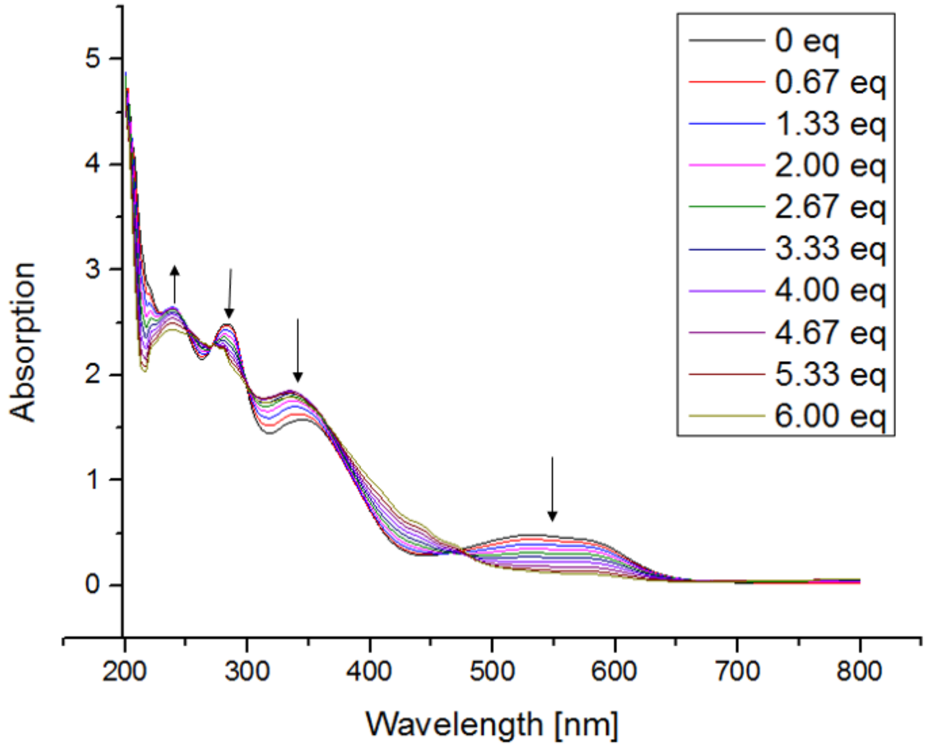

Figure S32: UV-Vis titration of **1** (3µM in CH_3CN) with sequential addition of $NOPF_6$.

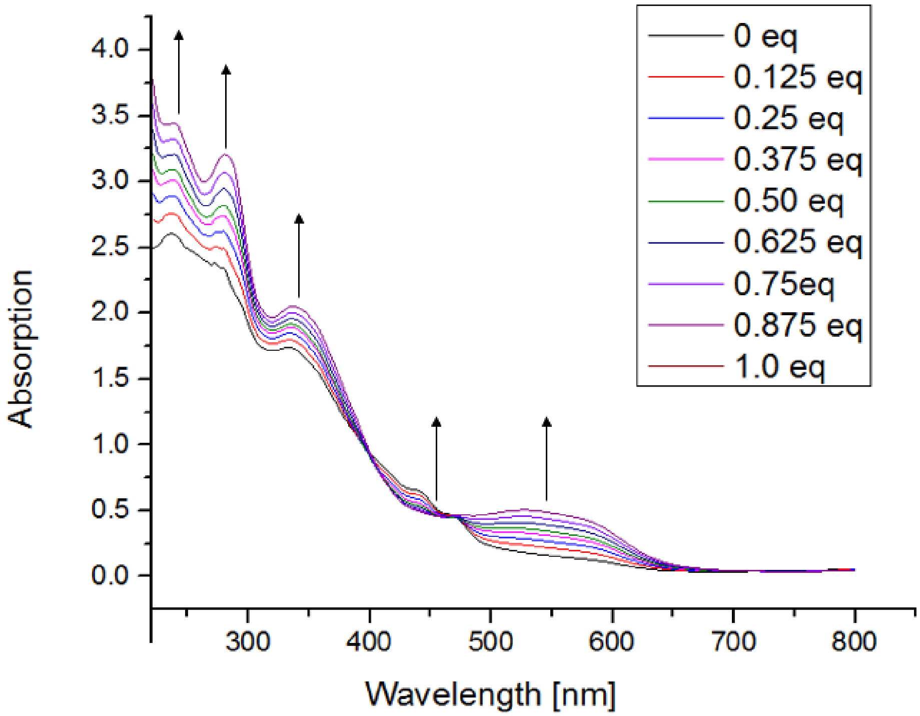

Figure S33: UV-Vis titration of **2** (12 µM in CH_3CN) with sequential addition of tetrakis(dimethylamine)ethylene.

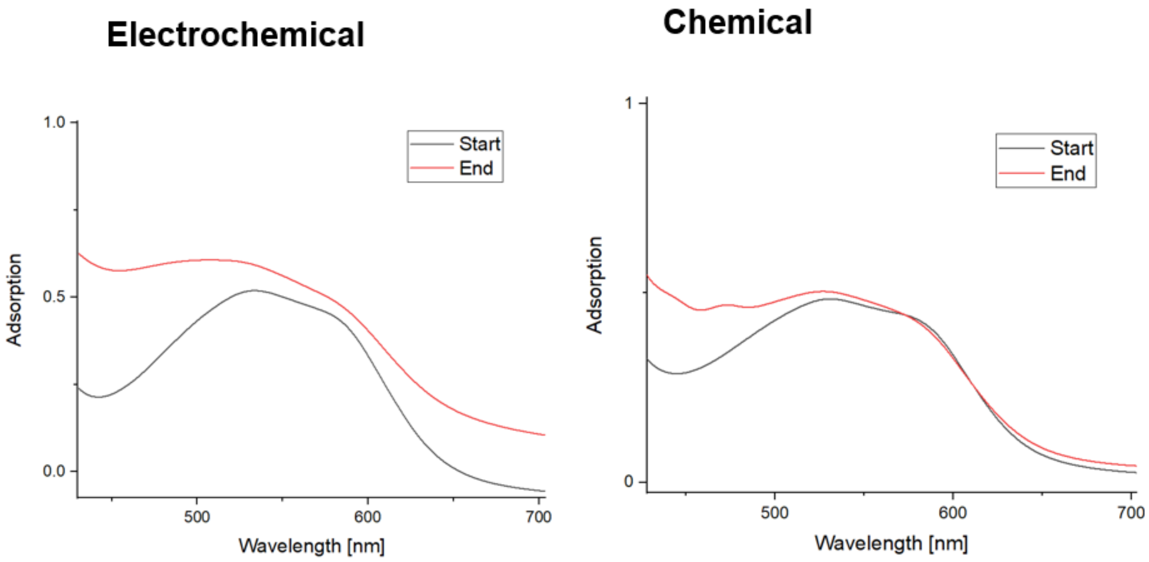

Figure S34: Comparison of the Fe^{II} MLCT bands after one cycle electrochemical and chemical oxidation and reduction (Start = **1**, End = after oxidation + reduction).

4.3 Determination of the magnetic moment of 2 using Evans' method

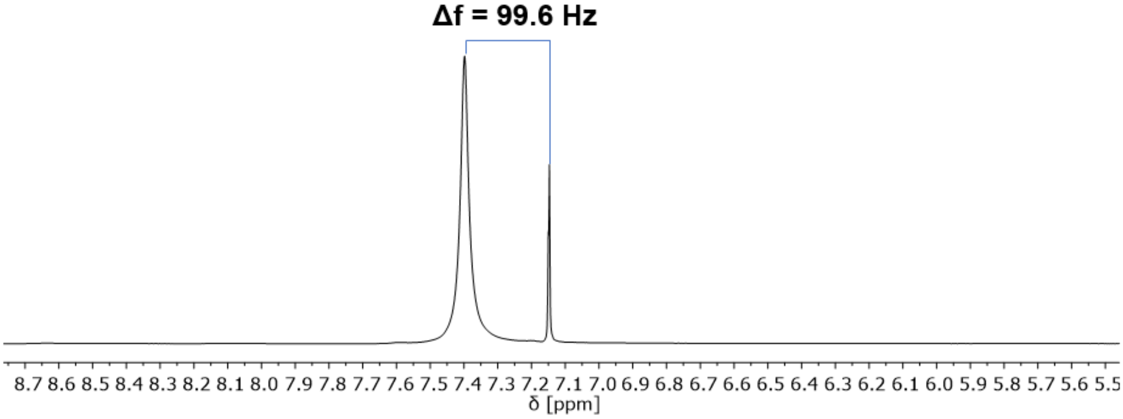

Figure SS35: Evans method using benzene as the shifted reagent by paramagnetic **2** in CD_3CN.

The magnetic susceptibility is calculated from:

$$\chi_M = (3\Delta f)/(4\pi F c)$$

with the difference between paramagnetically-shifted and unshifted benzene Δf = 99.6 Hz, the spectrometer frequency F = 400 MHz and the concentration of the paramagnetic complex c = n/V= $3.6\text{x}10^{-6}$ mol/ml (n = m/M; m = 2 mg, $Fe(L(PF_6)_3(CH_3CN)_2)$ = 1119 g/mol, V = 0.5 ml):

$$\chi_M = \ 0.0165\ cm^3/mol$$

Which gives a magnetic moment of

$$\mu = \sqrt{8\chi_M T} = 6.27\mu_B$$

with T = 298 K. This value compares well to the magnetic moment of 5 unpaired electrons $\mu = 5.92\mu_B$. No diamagnetic correction was applied.

5. Synthesis and Characterization of new compounds

5.1 Synthesis of mononuclear $[FeL_3](PF_6)_2$ complex

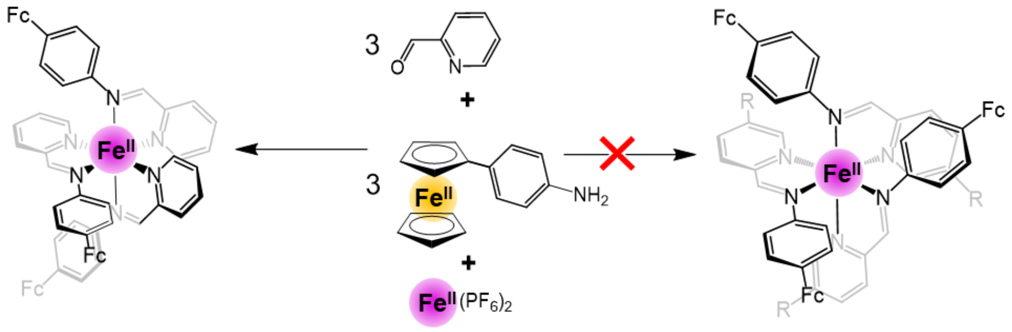

4-(aminophenylene)-ferrocene **B** (2.8 mg, 10 µmol), 2-pyridinecarboxaldehyde (1.2 mg, 10 µmol) and $Fe(PF_6)_2(CH_3CN)_6$ (2.0 mg, 3.3 µmol) were dissolved in CD_3CN (0.5 ml) and transferred into a J-Young NMR tube. The purple solution was subjected to three freeze-pump-thaw cycles under an N_2 atmosphere, and then heated at 50 °C for 16 h. The resulting purple solution was poured into 10 ml Et_2O to precipitate the product, which was isolated through centrifugation and dried under vacuum. Yield (5.1 mg, 2.9 µmol, 87%).

^{1}H NMR (CD_3CN, 400 MHz, 298 K): δ[ppm] = 9.37 (s, H-5), 9.10 (s, H-5), 8.98 (s, H-5), 8.57 (m, H-1, H-4), 8.42 (d, *J* = 5.8 Hz, H-4), 8.30 (t, *J* = 7.6 Hz, H-2), 8.13 (t, *J* = 7.1 Hz, H-2), 8.07 (d, *J* = 7.6 Hz, H-1), 8.00 (d, *J* = 7.1 Hz, H-1), 7.90 (t, *J* = 7.1 Hz, H-2), 7.76 (d, *J* = 4.9 Hz, H-4), 7.69 (t, *J* = 7.1 Hz, H-3), 7.69 (d, *J* = 7.1 Hz, H-3), 7.56 – 7.46 (m, H-3), 7.42 (d, *J* = 7.3 Hz, H-7), 7.31 (d, *J* = 5.9 Hz, H-7), 7.13 (d, *J* = 8.3 Hz, H-7), 6.78 – 6.58 (pt, *J* = 7.1 Hz, H-6, H-6), 6.21 (d, *J* = 7.4 Hz, H-6), 4.85 – 4.65 (m, H-8), 4.56 (d, *J* = 12.4 Hz, H-8), 4.52 – 4.27 (m, H-9), 4.08 (s, H-10), 3.92 (s, H-10), 3.91 (s, H-10).

^{13}C NMR (CD_3CN, 126 MHz, 298K): δ[ppm] = 174.31, 172.37, 171.19, 159.48, 158.88, 158.57, 157.08, 156.64, 155.91, 149.72, 145.46, 144.35, 141.37, 141.26, 140.83, 138.91, 138.81, 138.59, 131.60, 130.25, 129.93, 128.83, 128.70, 128.42, 126.67, 126.29, 125.99, 122.58, 122.12, 121.76, 69.75, 69.71, 69.67, 69.63, 69.60, 69.55, 66.69, 66.33, 65.86.

MS (ESI-MS, positive mode): m/z $[ML_3PF_6]^+$ (calcd. 1299.14): found 1298.93 $[ML_3]^{2+}$ (calcd. 577.09) found 577.06.

HRMS (ESI-MS, positive mode): m/z $[ML_3]^{2+}$ (calcd. 577.0901) found 577.0902.

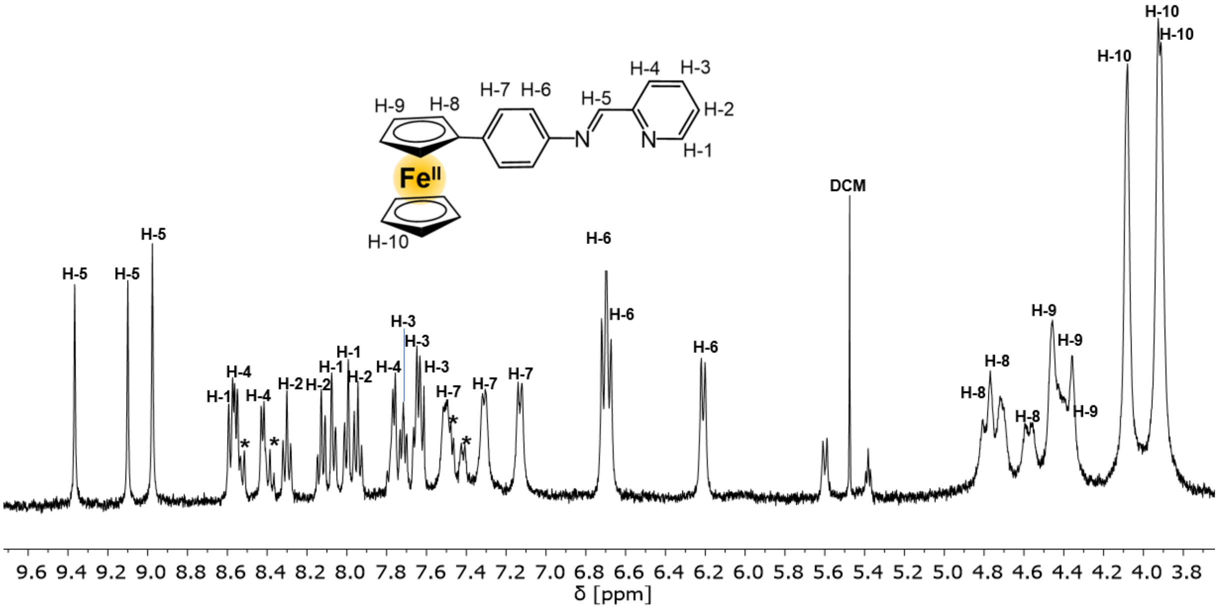

Figure S36: ^{1}H NMR spectrum (298K, CD_3CN, 400 MHz) of **$FeL^B_3(PF_6)_2$;** asterisks denote excess 2-pyridinecarboxaldehyde.

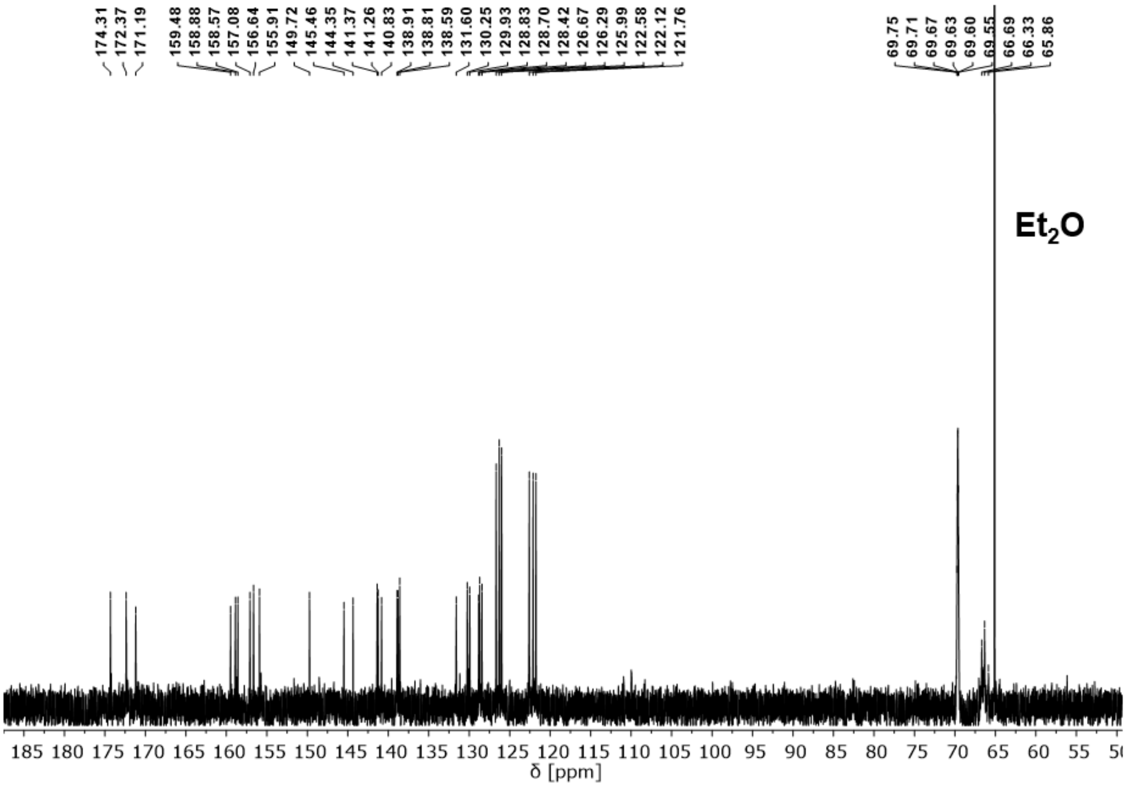

Figure S37: ^{13}C NMR spectrum **^{13}C NMR (CD_3CN, 126 MHz, 298K)** of **$FeL_3(PF_6)_2$**.

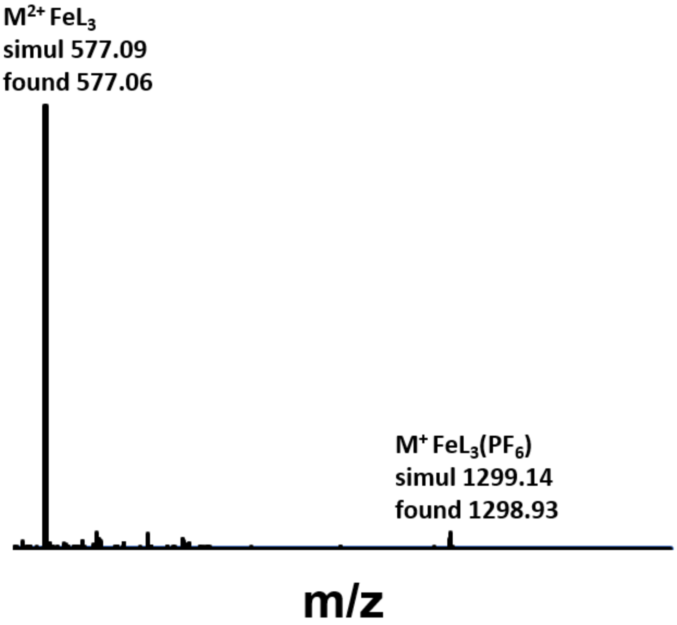

Figure S38: LR-ESI (positive mode) mass spectrum of **$FeL_3(PF_6)_2$**.

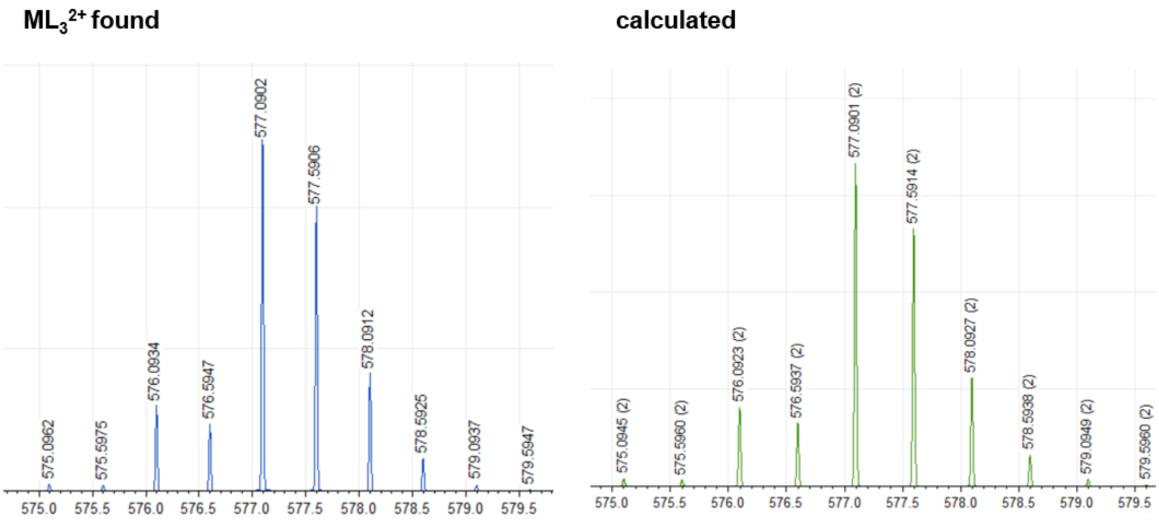

Figure S39: HRESI (positive mode) mass spectrum of the **FeL$_3^{2+}$** peak.

6. Crystallography

Data were collected at Beamline I19 of Diamond Light Source employing silicon double crystal monochromated synchrotron radiation (0.6889 Å) with ω scans at 100(2) K. Data integration and reduction for were undertaken with xia2[4]; multi-scan empirical absorption corrections were applied to the data using xia2[4]. Subsequent computations were carried out using the WinGX-32[5] graphical user interface. Structures were solved by direct methods using SHELXT-2013[6] then refined and extended with SHELXL-2013[6].

Crystal structure of 1·8NTf·5MeCN

Formula $C_{218}H_{159}F_{48}Fe_{10}N_{49}O_{32}S_{16}$, M 5960.39, Monoclinic , $P2_1/c$ (#16), a 26.651(5), b 27.050(5), c 36.959(7) Å, β 98.81(3), V 26330(9) Å^3, D_c 1.504 g cm^{-3}, Z 4, crystal size 0.200 by 0.200 by 0.150 mm, colour purple, habit block, temperature 100(2) Kelvin, λ(Synchrotron) 0.6889 Å, μ(Synchrotron) 0.767 mm^{-1}, T(Analytical)$_{\mathrm{min,max}}$ 0.9524, 1.0, $2\theta_{\mathrm{max}}$ 36.50, hkl range -24 24, -24 24, -32 33, N 98034, N_{ind} 20709(R_{merge} 0.1258), N_{obs} 12914(I > 2σ(I)), N_{var} 3364, residuals* $R1(F)$ 0.1492, $wR2(F^2)$ 0.3409, GoF(all) 1.059, $\Delta\rho_{\mathrm{min,max}}$ -0.548, 1.085 e$^-$ Å^{-3}, CCDC 2006764.

*$R1 = \Sigma||F_o| - |F_c||/\Sigma|F_o|$ for $F_o > 2\sigma(F_o)$; $wR2 = (\Sigma w(F_o^2 - F_c^2)^2/\Sigma(wF_c^2)^2)^{1/2}$ all reflections $w=1/[\sigma^2(F_o^2)+(0.0500P)^2+400.0000P]$ where $P=(F_o^2+2F_c^2)/3$

Specific refinement details

Crystals of **$Fe_4L^{azo}_6$·8NTf$_2$·5MeCN** were grown by slow diffusion of diethyl ether into a CD_3CN solution of **$Fe_4L^{azo}_6(NTf_2)_8$**. Despite the use of synchrotron radiation, few reflections at greater than 1.1 Å resolution were observed. Nevertheless, the quality of the data is more than sufficient to establish the connectivity of the structure.

The crystals employed in this study rapidly lost solvent after removal from the mother liquor and rapid handling prior to flash cooling in the cryostream was required to collect data. Due to the less than ideal resolution, bond lengths and angles within pairs of organic ligands were restrained to be similar to each other (SAME) and thermal parameter restraints (SIMU, DELU) were applied to all non-metal atoms to facilitate anisotropic refinement. Ligand-based atoms that still displayed thermal parameters greater than 0.4 were further refined to approximate isotropic behavior (ISOR). Four triflimide anions were modelled as disordered over two positions.

In general, non-hydrogen atoms with occupancies greater than 0.5 were refined anisotropically. Carbon-bound hydrogen atoms were included in idealized positions and refined using a riding model. Disorder was modelled using standard crystallographic methods including constraints, restraints and rigid bodies where necessary. The amount of solvent quoted in the molecular formula is only that which could be assigned directly from the electron density map.

The SQUEEZEd portion of the cell totals 856 electrons per unit cell, with a solvent accessible void volume of 2,917 Å^3 per unit cell. This equates to 214 electrons per structure, where $Z = 4$. As all NTf_2^- molecules were resolved, we attribute this excess electron density to unresolved solvent molecules (Et_2O and MeCN).

CheckCIF produces 1 Level A and 4 Level B alerts. These alerts are due to the high thermal motion of some atoms in the crystal (particularly the sulfur atoms of the triflimide anions), leading to the less than ideal resolution of the data.

7. References

[1] E. C. Taylor, C. P. Tseng, J. B. Rampal, *The Journal of Organic Chemistry* **1982**, *47*, 552-555.

[2] M. Qi, Y. Zhang, C. Cao, M. Zhang, S. Liu, G. Liu, *Analytical Chemistry* **2016**, *88*, 9614-9621.

[3] D. D. Swanson, K. M. Conner, S. N. Brown, *Dalton Transactions* **2017**, *46*, 9049-9057.

[4] a) P. R. Evans, G. N. Murshudov, *Acta Crystallogr. Sect. D* **2013**, *69*, 1204-1214; b) G. Winter, *J. Applied Cryst.* **2010**, *43*, 186-190.

[5] L. Farrugia, *J. Applied Cryst.* **2012**, *45*, 849-854.

[6] G. M. Sheldrick, *Acta Crystallogr. Sect. A* **2015**, *71*, 3-8.